NATIONAL ADVISORY COMMITTEE FOR AERONAUTICS

WARTIME REPORT

ORIGINALLY ISSUED

December 1944 as
Advance Restricted Report L4K22a

THE CONFORMAL TRANSFORMATION OF AN AIRFOIL INTO A STRAIGHT LINE AND ITS APPLICATION TO THE INVERSE PROBLEM OF AIRFOIL THEORY

By William Mutterperl

Langley Memorial Aeronautical Laboratory
Langley Field, Va.

NACA

WASHINGTON

NACA ARR No. L4K22a [redacted]

NATIONAL ADVISORY COMMITTEE FOR AERONAUTICS

ADVANCE RESTRICTED REPORT

THE CONFORMAL TRANSFORMATION OF AN AIRFOIL INTO A STRAIGHT LINE AND ITS APPLICATION TO THE INVERSE PROBLEM OF AIRFOIL THEORY

By William Mutterperl

SUMMARY

A method of conformal transformation is developed that maps an airfoil into a straight line, the line being chosen as the extended chord line of the airfoil. The mapping is accomplished by operating directly with the airfoil ordinates. The absence of any preliminary transformation is found to shorten the work substantially over that of previous methods. Use is made of the superposition of solutions to obtain a rigorous counterpart of the approximate methods of thin-airfoil theory. The method is applied to the solution of the direct and inverse problems for arbitrary airfoils and pressure distributions. Numerical examples are given. Applications to more general types of regions, in particular to biplanes and to cascades of airfoils, are indicated.

INTRODUCTION

In an attempt to set up an efficient numerical method for finding the potential flow through an arbitrary cascade of airfoils (reference 1) a method of conformal transformation was developed that was found to apply to advantage in the case of isolated airfoils.

The method consists in transforming the isolated airfoil directly to a straight line, namely, the extended chord line of the airfoil. The absence of the hitherto usual preliminary transformation of the airfoil into a near circle makes for a decided simplification of concept and procedure.

[redacted]

The exposition of the method, followed by its application to the direct problem of the conformal mapping of given airfoils, is given in part I of this paper. In part II the method is applied to the inverse problem of airfoil theory; namely, the derivation of an airfoil section to satisfy a prescribed velocity distribution. A comparison with previous inverse methods is made. Additional material that will be of use in the application of the method is given in the appendixes. In appendix A certain numerical details of the calculations are discussed. In appendix B extensions of the method to the conformal mapping of other types of regions are indicated. The relation of the methods used for the mapping of airfoils to the Cauchy integral formula is discussed in appendix C.

Acknowledgment is made to Mrs. Lois Evans Doran of the computing staff of the Langley full-scale tunnel for her assistance in making the calculations.

SYMBOLS

$z = x + iy$ plane of airfoil

$\zeta = \xi + i\eta$ plane of straight lines

p plane of unit circle

φ central angle of circle

Δx component of Cartesian mapping function (CMF) parallel to chord

Δy component of Cartesian mapping function perpendicular to chord

Δx_o, Δy_o particular CMF's, tables I and II

τ displacement constant for locating airfoil

$r = 2R$ diameter of circle, semilength of straight line

$c_n = a_n + ib_n$ coefficients of series for CMF

β_N negative of central angle of circle, corresponding to leading edge of airfoil

β_T central angle of circle minus 180°, corresponding to trailing edge of airfoil

c airfoil chord

c_l section lift coefficient

v_z velocity at surface of airfoil, fraction of free-stream velocity

v_p velocity at surface of circle, fraction of free-stream velocity

V free-stream velocity

ds element of length on airfoil

Γ circulation

u_t thickness factor

u_c camber factor

T thickness ratio

λ normalizing constant

k denominator of equation (17)

C camber, percent

δx, δy incremental CMF's

U positive area under approximate $v_p(\varphi)$ curve

L negative area under approximate $v_p(\varphi)$ curve

α angle of attack

α_I ideal angle of attack

$\gamma = \alpha + \beta_T$

Φ_t true potential

Φ_a approximate potential

θ central angle of near circle

$\epsilon = \varphi - \theta$

Subscripts:

N leading edge (nose)

T trailing edge

c camber

t thickness

o, 1, 2 successive approximation in direct or inverse CMF methods

I - THE DIRECT POTENTIAL PROBLEM OF AIRFOIL THEORY

THE CARTESIAN MAPPING FUNCTION

The Derivation of the Cartesian Mapping Function

Consider the transformation of an airfoil, z-plane, into a straight line, ζ-plane (fig. 1). The vector distance between conformally corresponding points such as P_z and P_ζ on the two contours is composed of a horizontal displacement Δx and a vertical displacement Δy. The quantity $\Delta x + i\,\Delta y$ is only another way of writing the analytic function $z - \zeta$; that is,

$$
\begin{aligned}
z - \zeta &= (x + iy) - (\xi + i\eta) \\
&= (x - \xi) + i(y - \eta) \\
&\equiv \Delta x + i\,\Delta y \qquad (1)
\end{aligned}
$$

By Riemann's basic existence theorem on conformal mapping, the function $z - \zeta$ connecting conformally corresponding points in the z- and ζ-planes is a regular function of either z or ζ everywhere outside the airfoil or straight line. This function will be referred to as a Cartesian mapping function, or CMF. In order to map an airfoil onto a straight line, the airfoil ordinates Δy are regarded as the imaginary part of an analytic function on the straight line and the problem reduces to the calculation of the real part Δx.

The calculation of the real part of an analytic function on a closed contour from the known values of the imaginary part is well known. It is convenient for this calculation to consider the straight line as conformally related to a circle, p-plane, by the familiar transformation

$$\zeta - \tau = p + \frac{R^2}{p} \tag{2a}$$

where the constant displacement τ has been inserted for future convenience in locating the airfoil. For corresponding points on the straight line and the circle, equation (2a) reduces to

$$\left.\begin{aligned} \xi &= \tau + r\cos\varphi \\ \eta &= 0 \end{aligned}\right\} \tag{2b}$$

Considered as a function of p, therefore, the CMF $z - \zeta$ is regular everywhere outside the circle and is therefore expressible by the inverse power series:

$$z - \zeta = \sum_{0}^{\infty} \frac{c_n}{p^n} \tag{3}$$

The analogy of equation (3) with the Theodorsen-Garrick transformation (reference 2)

$$\log \frac{p'}{p} = \sum_{1}^{\infty} \frac{c_n}{p^n}$$

which relates conformally a near circle, p'-plane, to a circle, p-plane, may be noted. On the circle proper, where $p = Re^{i\varphi}$, and defining $c_n \equiv a_n + ib_n$, equation (3) reduces to two conjugate Fourier series for the CMF; namely,

$$\Delta x = a_o + \sum_{1}^{\infty} \frac{a_n}{R^n} \cos n\varphi + \sum_{1}^{\infty} \frac{b_n}{R^n} \sin n\varphi \tag{4}$$

$$\Delta y = b_0 + \sum_1^\infty \frac{b_n}{R^n} \cos n\varphi - \sum_1^\infty \frac{a_n}{R^n} \sin n\varphi \qquad (5)$$

These series evidently determine Δx from Δy or vice versa.

An alternative method of performing this calculation is possible. It is known that if the real and imaginary parts of a function are given by conjugate Fourier series, as in equations (4) and (5), with the constant terms zero, two integral relations are satisfied. (See, for example, references 2 and 3; also, appendix C.) These relations are

$$\Delta x(\varphi) = -\frac{1}{2\pi}\int_0^{2\pi} \Delta y(\varphi') \cot \frac{\varphi' - \varphi}{2} \, d\varphi' \qquad (6)$$

$$\Delta y(\varphi) = \frac{1}{2\pi}\int_0^{2\pi} \Delta x(\varphi') \cot \frac{\varphi' - \varphi}{2} \, d\varphi' \qquad (7)$$

Before the detailed application of the CMF $z - \zeta$ to the solution of the direct and inverse problems of airfoil theory is made, some necessary basic properties of this function will be discussed.

Airfoil Position for Given CMF

It is noted first that the regions at infinity in the three planes are the same except for a trivial and arbitrary translation; that is, by equations (1), (2a), and (3),

$$\left.\begin{aligned} &\lim_{z,\zeta\to\infty} z - \zeta \equiv \Delta x_\infty + i\,\Delta y_\infty = c_0 \equiv a_0 + ib_0 \\ &\lim_{\zeta, p\to\infty} \zeta = p + \tau \end{aligned}\right\} \qquad (8)$$

Secondly, if an airfoil is to be mapped into a straight line, it becomes necessary to know the point on the straight line corresponding to the trailing edge of the airfoil. For a given CMF, $\Delta x(\varphi)$, $\Delta y(\varphi)$, and straight line of length $2r$ located as in figure 1, the airfoil coordinates x, y are obtained from equations (1) and (2b) as

$$x = \tau + r \cos \varphi + \Delta x(\varphi) \tag{9}$$

$$y = \Delta y(\varphi) \tag{10}$$

The leading and trailing edges of the airfoil will be taken as the points corresponding to the extremities of the airfoil abscissas. The corresponding locations on the circle are therefore determined by maximizing x with respect to φ in equation (9). Thus

$$\frac{dx}{d\varphi} = 0 = -r \sin \varphi + \frac{d\Delta x}{d\varphi}$$

or

$$\sin \varphi = \frac{d\Delta x}{r\, d\varphi} \tag{11}$$

The condition (11) yields (usually by graphical determination) the angles corresponding to the leading and trailing edges (fig. 1)

$$\left.\begin{aligned} \varphi_N &\equiv -\beta_N \\ \varphi_T &\equiv \pi + \beta_T \end{aligned}\right\} \tag{12}$$

It will be found convenient to so alter the position and scale of a derived airfoil that, for example, its chordwise extremities are located at $x = \pm 1$ and the trailing edge has the ordinate $y = 0$ (to be referred to as the normal form). The chord c of a derived airfoil is by definition the difference in airfoil abscissa extremities, or by equations (12) and (9),

$$c = r\left(\cos \beta_N - \cos \beta_T\right) + \Delta x\left(\varphi_N\right) - \Delta x\left(\varphi_T\right) \tag{13}$$

The increase in scale from c to some desired c_o is obtained simply by multiplying r, Δx, and Δy by the factor c_o/c. The translation necessary to bring the trailing edge of the airfoil to its desired location is then accomplished by adjusting the translation constants τ and b_o.

Velocity Distribution on Airfoil

Once the CMF $\Delta x(\varphi)$, $\Delta y(\varphi)$ and the diameter of circle r of an airfoil have been determined, the velocity at a point on its surface is obtained in a well-known manner as the product of the known velocity at the corresponding point of the circle and the stretching factor from the circle to the airfoil; that is,

$$v_z(\varphi) = r \frac{d\varphi}{ds} v_p(\varphi) \tag{14}$$

where $v_p(\varphi)$ is half the velocity on the circle (since $r = 2R$) and ds is the element of length on the airfoil.

The velocity on the circle $v_p(\varphi)$, which makes the point $\varphi = \pi + \beta_T$ corresponding to the trailing edge of the airfoil a stagnation point (Kutta condition), is

$$v_p(\varphi) = \left|\sin(\varphi + \alpha) + \sin\left(\alpha + \beta_T\right)\right| \tag{15}$$

where α is the angle of attack. The velocities v_p and v_z are expressed nondimensionally as fractions of free-stream velocity. The stretching factor $ds/d\varphi$ is obtained from equations (9) and (10) as

$$\frac{ds}{d\varphi} = \sqrt{\left(\frac{dx}{d\varphi}\right)^2 + \left(\frac{dy}{d\varphi}\right)^2} = \sqrt{\left(\frac{d\Delta x}{d\varphi} - r \sin\varphi\right)^2 + \left(\frac{d\Delta y}{d\varphi}\right)^2} \tag{16}$$

The velocity $v_z(\varphi)$, equation (14), therefore becomes

$$v_z(\varphi) = \frac{\left|\sin(\varphi + \alpha) + \sin\left(\alpha + \beta_T\right)\right|}{\sqrt{\left(\frac{d\Delta x}{r\, d\varphi} - \sin\varphi\right)^2 + \left(\frac{d\Delta y}{r\, d\varphi}\right)^2}} \tag{17}$$

This equation is the general expression, in terms of the CMF, for the velocity at the surface, equations (9) and (10), of an arbitrary airfoil. The denominator depends only on the airfoil geometry, while the numerator depends also on the angle of attack. Equation (17) is similar to the corresponding expression in the Theodorsen-Garrick method except for the absence of the factor representing a preliminary transformation from the airfoil to a near circle.

The expressions for the lift coefficient and ideal angle of attack may be noted. The circulation Γ around the airfoil is (V is free-stream velocity)

$$\Gamma = 4\pi RV \sin\left(\alpha + \beta_T\right) \tag{18}$$

The lift coefficient c_l is defined by

$$\frac{1}{2} cc_l V \equiv \Gamma$$

Hence

$$c_l = 4\pi \frac{r}{c} \sin\left(\alpha + \beta_T\right) \tag{19}$$

where the airfoil chord c is given by equation (13).

The ideal angle of attack (reference 2) is defined as that angle of attack for which a stagnation point exists at the leading edge; that is, $v_z = 0$ for $\varphi = -\beta_N$ in equation (17). Hence,

$$\alpha_I = \frac{\beta_N - \beta_T}{2} \tag{20}$$

Superposition of Solutions

The sum of two analytic functions is an analytic function; therefore, for a given p-plane circle, the sum of two CMF's is itself a CMF as is also evident from equations (4) to (7). Thus, the CMF's $\Delta x_1 + i\,\Delta y_1$ and $\Delta x_2 + i\,\Delta y_2$ of two component airfoils may, for the same r, be added together to give a CMF $\left(\Delta x_1 + \Delta x_2\right) + i\left(\Delta y_1 + \Delta y_2\right)$ and thence, by equation (17), an exact velocity distribution for a resultant airfoil. The resultant profile and its velocity distribution is a superposition in this sense of the component profiles and velocity distributions. Thus, without sacrifice of exactness and with no great increase of labor, airfoils may be analyzed and synthesized in terms of component symmetrical thickness distributions and mean camber lines. This result provides a rigorous counterpart of the well-known approximate superposition methods of thin-airfoil vortex and source-sink potential theory.

As a particular case of superposition, a known CMF $\Delta x + i\,\Delta y$ may be multiplied by a constant S and the resulting CMF $S\,\Delta x + iS\,\Delta y$ determines a new profile by the new displacements $S\,\Delta x$, $S\,\Delta y$ from points on the original straight line. It is evident that, except for the corrections $(S - 1)\,\Delta x$ to the airfoil abscissas, this new profile is increased in thickness and camber over the original profile by the factor S. The effect on the velocity distribution is that of multiplying the derivatives in equation (17) by S. By virtue of a reduction in scale by the factor $1/S$ this profile may also be regarded as obtained from the original one by using the same Δx, Δy but a length of line $1/S$ times the length of the original one.

The use of superposition as well as the application of the CMF to some particular airfoils will be illustrated next.

Application of the CMF to Some Particular Airfoils

Symmetrical thickness distributions.- The Cartesian mapping function was calculated for a symmetrical 30-percent thickness ratio Joukowski profile from the known conformal correspondence between a Joukowski profile and a straight line. The CMF is given in normal form in table I. The associated constants τ_o and r_o are given in table II and the profile itself, as determined either from the standard formulas or from equations (9) and (10), is shown in figure 2(a). The symmetry of the profile required only the calculation of $\Delta x(\varphi)$, $\Delta y(\varphi)$ for $0 \leq \varphi \leq 180^\circ$. The corresponding velocity distribution (fig. 2(b)) was obtained from equation (17) by use of the computed values of the derivatives. At the cusped trailing edge the velocity as given by equation (17) is indeterminate; however, the limiting form of equation (17), determined by differentiation of numerator and denominator, is

$$\lim_{\varphi \to \varphi_T} v = \frac{\left|\cos\,(\varphi + \alpha)\right|}{\sqrt{\left(\cos\,\varphi - \dfrac{d^2\Delta x}{r\,d\varphi^2}\right)^2 + \left(\dfrac{d^2\Delta y}{r\,d\varphi^2}\right)^2}} \tag{21}$$

It is seen from this expression that the velocity at a cusped edge depends on the second derivatives of the mapping function, that is, on the curvature at the cusp. The computed second derivatives $d^2\Delta x_{ot}/d\varphi^2$, $d^2\Delta y_{ot}/d\varphi^2$ of the CMF of table I are plotted in figure 3 for a range of values of φ near 180°.

The CMF's for symmetrical profiles of different thickness ratios were determined from that for the Joukowski profile as indicated previously in the section "Superposition of Solutions." The factor u_t by which to multiply Δx_o, Δy_o to obtain a profile of thickness ratio T is obtained from

$$\frac{u_t \, \Delta y_{o_{max}}}{r_o + u_t \dfrac{\left[\Delta x(\varphi_N) - \Delta x(\varphi_T)\right]}{2}} = T$$

where Δy_o is the maximum airfoil ordinate of the known CMF (table I) and the denominator represents the semichord of the derived profile. The solution for u_t is

$$u_t = \frac{r_o T}{\Delta y_{o_{max}} + T\left(\dfrac{\Delta x_T - \Delta x_N}{2}\right)} \tag{22}$$

Values of u_t were calculated from this formula for thickness ratios of 24 percent and 12 percent and are given in table II. The resulting CMF's were then normalized as indicated in the section "Airfoil Position for Given CMF" so that the actual factors by which to multiply the original Δx_o, Δy_o were λu_t. These values are given in table II, together with the associated constants τ and r. The profiles thus determined are shown in figure 2(a) and the corresponding velocity distributions in figure 2(b).

The derived profiles are not Joukowski profiles. The point of maximum thickness is shifted back along the chord somewhat as the thickness ratio decreases. Conversely, the point of maximum thickness would be shifted forward by going from a thin Joukowski profile to a thicker one. (This result was the reason for starting from a thick section.) The CMF for the 12-percent thick derived profile is illustrated in figure 4. It is to be noted that the horizontal displacement function $\Delta x_{ot}(\varphi)$ is symmetrical about $\varphi = \pi$, whereas the vertical displacement function $\Delta y_{ot}(\varphi)$ is antisymmetrical about $\varphi = \pi$.

Mean camber lines.- The CMF was next calculated for a circular-arc profile of 6-percent camber from the known conformal correspondence between a circular arc and a straight line. The normalized CMF and its derivatives are given in table III. The CMF is illustrated in figure 4. The symmetry in this case is with respect to $\varphi = 90^\circ$ and $\varphi = 270^\circ$, the $\Delta x_{oc}(\varphi)$ being antisymmetrical and $\Delta y_{oc}(\varphi)$ symmetrical. The circular-arc mean camber line is shown in figure 5(a) and the corresponding velocity distribution in figure 5(b).

Derived mean camber lines were obtained from the CMF for the circular arc in a manner similar to that for the symmetrical profiles. The expression determining the factor u_c for a desired percent camber C is

$$\frac{u_c \ \Delta y_{o_{max}}}{2\left[r_o \cos \varphi_N + u_c \ \Delta x\left(\varphi_N\right)\right]} = C$$

with the solution for u_c

$$u_c = \frac{2Cr_o \cos \varphi_N}{\Delta y_{o_{max}} - 2C \ \Delta x\left(\varphi_N\right)} \tag{23}$$

The angle φ_N in equation (23) (as in equation (22)) corresponds to the extremity of the derived mean line. Because the factor u_c is to multiply the derivative $d\Delta x_o(\varphi)/d\varphi$, the angle φ_N as determined by the maximum condition (11) depends on u_c. One or two trials are sufficient to determine u_c simultaneously with φ_N from equations (23) and (11) for a given desired camber C. Values of u_c and φ_N (also φ_T by symmetry) are given in table IV for derived cambers of 3 and 9 percent. The actual multiplying factor to obtain the derived CMF's in normal form is given in table IV as λu_c.

The derived camber lines are shown in figure 5(a). It is seen that the derived camber lines have been separated into distinct upper and lower surfaces. Furthermore, for the 9-percent camber line the "lower" surface, that is, the surface corresponding to the lower part of the straight line or circle, lies above the "upper" surface. Although such a camber line is physically meaningless by itself, nevertheless its CMF can be compounded with that for a thickness distribution to give a physically real result (if the resultant profile is a real one). The velocity distribution of the 3-percent camber line is given in figure 5(b). The "velocity distribution" of the 9-percent camber line is included in figure 5(b) for arithmetical comparison although it is physically meaningless for the reason just mentioned.

The velocities at the cusped extremities of the camber lines are given by equation (21). The second derivatives of the CMF of table III were computed. They are plotted in figure 3 as $d^2\Delta x_{oc}/d\varphi^2$, $d^2\Delta y_{oc}/d\varphi^2$ for a range of φ near 180°. These second derivatives, in combination with those for the symmetrical profile, can be used to give a more accurate determination of the velocity at and near a cusped trailing edge than is obtained by using equation (17) near the trailing edge.

Combination of symmetrical profile and mean camber line.- The CMF's derived for the symmetrical profiles and for the mean camber lines can now be combined in varying proportions to produce airfoils having both thickness and camber. These airfoils may be useful in themselves or, as in the following sections, may be used as initial approximations in both the direct and inverse processes.

As an illustration of such combinations, the CMF of the 12-percent thick symmetrical profile of figure 2(a) and the CMF of the 6-percent camber circular arc of figure 5(a) were added together. The airfoil profile thus determined is shown in figure 6(a). For comparison, the airfoil obtained in the manner of thin-airfoil theory (see, for example, reference 4) by superposition of the same symmetrical profile and a 6.5-percent camber circular arc (in order to duplicate the camber of the exact airfoil more closely) is indicated in the figure. The velocity distribution of the dotted airfoil should, according to thin-airfoil theory, be the sum of the symmetrical-profile velocity and the increment above the free-stream value of the camber-line velocity. This velocity distribution, determined from the two component exact distributions at zero angle of attack, is shown dotted in figure 6(b). The exact velocity distribution of the "exact" airfoil of figure 6(a) was determined for the same lift coefficient ($c_l = 0.88$, $\alpha = 1^{\circ}13'$) from the known CMF. This distribution is shown in figure 6(b). The two velocity distributions differ appreciably, although in the directions to be expected from the differences in shape of the corresponding airfoils.

It appears that the CMF's of a relatively small number of useful thickness distributions and camber lines would suffice to yield a large number of useful combinations of which the (perfect fluid) characteristics could be determined exactly and easily in the manner indicated.

The superposition of solutions can also be used with the airfoil mapping methods based on the conformal transformation of a near circle to a circle. There is a decided advantage, however, in working with the airfoil ordinates directly, both in the facility of the calculations and in the insight that is maintained of the relationship between an airfoil and its velocity distribution.

THE DIRECT POTENTIAL PROBLEM FOR AIRFOILS

The direct problem for airfoils is that of finding the potential flow past a given arbitrary airfoil section situated in a uniform free stream. This problem can be solved by a CMF method of successive approximation somewhat similar to that in reference 2.

Method of Solution

Suppose an airfoil to be given as in figure 6(a). The chord is taken as any straight line such that perpendiculars drawn from its extremities are tangent to the airfoil. For example, the "longest-line" chord, that is, the longest line that can be drawn within the airfoil, satisfies this definition. The x-axis is taken along this chord and the origin is taken at its midpoint. Suppose, in addition, an initial CMF Δx_0 and Δy_0, straight line r_o, and chordwise translation constant τ_o to be given such that the corresponding airfoil has the same chord and is similar in shape to the given airfoil. (At the worst the initial airfoil could be the given chord line itself.)

At the chordwise locations $x_o(\varphi)$ of the initial airfoil, corresponding to an evenly spaced set of φ-values by equation (9), the differences $\delta y_1(\varphi)$ between the ordinates $\Delta y_1(\varphi)$ of the given airfoil and $\Delta y_o(\varphi)$ of the initial airfoil are measured. The ordinate differences $\delta y_1(\varphi)$ determine a conjugate set of abscissa corrections $\delta x_1(\varphi)$ in accordance either with equations (4) and (5) or equation (6). The details of this calculation are given in appendix A.

The initial semilength of straight line r_o corresponding to the initial airfoil is then corrected to r_1, and the translation constant τ_o adjusted to τ_1, so that the use of r_1 with the first approximate CMF $\Delta x_1 = \Delta x_o + \delta x_1$, $\Delta y_1 = \Delta y_o + \delta y_1$ yields a first approximate airfoil of which the chordwise extremities coincide with those of the given airfoil. This correction is described in detail presently. If the first approximate airfoil is not satisfactorily close to the given airfoil, the procedure is repeated for a second approximate airfoil, and so on. The successive airfoils thus determined provide a very useful criterion of convergence to the final solution; namely, the given airfoil. Evidently, the fundamental relation between an airfoil and its mapping circle

$$z - p = c_o + \frac{c_1}{p} + \frac{c_2}{p^2} + \ldots$$

can be used in the manner indicated to effect directly the transformation of an airfoil into a circle. It appears preferable, however, to subtract R^2/p from the second term on the right and thence to introduce the straight-line variable $\zeta = p + \frac{R^2}{p}$.

The exact velocity distribution of any of the "approximate" airfoils (hence the approximate velocity distribution of the given airfoil) may be obtained from equation (17) using the derivatives of the corresponding CMF. The zero-lift angle β_T to be used in equation (17) is determined for each approximate airfoil along with the corresponding correction for r.

The correction for r is necessary because if the chordwise locations of the first approximate airfoil were computed by equation (9) with the original values of r and τ, $\Delta x_1(\varphi)$ being used instead of $\Delta x_0(\varphi)$, the resulting chordwise extremities would in general not be at $x = \pm 1$. It is therefore necessary to adjust r_0 and τ_0 such that with the derived Δx_1, Δy_1,

$$\left.\begin{aligned} x_1\left(\varphi_{N_1}\right) &= 1 \\ x_1\left(\varphi_{T_1}\right) &= -1 \end{aligned}\right\} \tag{24}$$

where φ_{N_1} and φ_{T_1} are the angles on the circle corresponding to the extremities of the desired airfoil. This operation was mentioned in the section "Superposition of Solutions." It may be termed a horizontal stretching of the given airfoil. The condition given by equations (24) applied to equation (9) yields

$$\left.\begin{aligned} 1 &= \tau_1 + r_1 \cos \varphi_{N_1} + \Delta x_1\left(\varphi_{N_1}\right) \\ -1 &= \tau_1 + r_1 \cos \varphi_{T_1} + \Delta x_1\left(\varphi_{T_1}\right) \end{aligned}\right\} \tag{25}$$

Subtraction of the second of these equations from the first gives for r_1

$$r_1 = \frac{1 + \dfrac{\Delta x_1\left(\varphi_{T_1}\right) - \Delta x_1\left(\varphi_{N_1}\right)}{2}}{\dfrac{\cos \varphi_{N_1} - \cos \varphi_{T_1}}{2}} \tag{26}$$

Addition of equations (25) gives for τ_1

$$\tau_1 = -\left[r_1 \frac{\cos \varphi_{N_1} + \cos \varphi_{T_1}}{2} + \frac{\Delta x\left(\varphi_{N_1}\right) + \Delta x_1\left(\varphi_{T_1}\right)}{2}\right] \tag{27}$$

The angles φ_{N_1} and φ_{T_1} in equations (26) and (27) correspond to the extremities of the desired airfoil. They are given by graphical solution of equation (11)

$$\sin \varphi = \frac{d\Delta x_1(\varphi)}{r_1 \, d\varphi} \tag{11}$$

Equation (11) must be solved simultaneously with equation (26) for r_1, φ_{N_1}, and φ_{T_1}. In practice only a few successive trials are necessary. Thence τ_1 is obtained by equation (27). The angle φ_{T_1} determined in this process is equivalent to the zero-lift angle of the airfoil, equation (12).

Illustrative Example of Direct Method

As a numerical illustration of the direct method the velocity distribution of the NACA 6512 airfoil was calculated. In order to obtain an initial airfoil, the CMF of the 6-percent camber circular arc (tables III and IV) was added to the CMF of the 12-percent thick symmetrical profile, derived from that of table I as indicated in a previous section. Before this addition was made, the CMF for the circular arc was increased in scale (multiplied) by 1.0928/1.0072 to correspond to the same length of straight line r as the symmetrical profile CMF. The normalized resultant CMF and the associated constants are given in tables V(a) and VI, respectively. The initial airfoil is shown in figure 7(a).

The given airfoil, NACA 6512, was so rotated through an angle of -0.88° (nose down) as to be tangent to the initial airfoil at the leading edge. The convergence near the leading edge was thereby accelerated. The given airfoil is shown in this position in figure 7(a). Two approximations were then carried out in accordance with the procedure given in the preceding section. The numerical results are given in tables V and VI. The first approximate airfoil is indicated by the circles in figure 7(a); the second approximate airfoil was indistinguishable to the scale used (chord = 20 in.) from the given airfoil. The velocity distributions of the initial, first, and second approximate airfoils are given in figure 7(b), together with those corresponding to one approximation by the Theodorsen-Garrick method (reference 5). The second approximation velocity distribution differs appreciably from that of the Theodorsen-Garrick method on the upper surface but agrees fairly well on the lower surface. The discrepancy for the rearmost 5 percent of chord on the lower surface appears to be due to lack of detail in this region in the Theodorsen-Garrick calculation.

The convergence of the CMF method is seen to be rapid, considering the approximate nature of the initial airfoil, although two approximations are required for a satisfactory result. The second approximation could probably have been made unnecessary by suitably adjusting the first increment $\delta y_1(\varphi)$ near the leading and trailing edges on the upper surface before calculating $\delta x_1(\varphi)$. The direction in which to adjust the increment is obtained by comparing the thickness of the initial airfoil with that of the given airfoil in these regions. Because a thicker section has a greater concentration of chordwise locations toward the extremities, for a given set of φ points, than does a thinner section, the chordwise stations would be expected to be shifted outward as the thickness of the section is increased. The ordinates $\Delta y_1(\varphi)$ should therefore have been chosen at chordwise stations slightly more toward the extremities than those given by equation (9).

The accuracy of the velocities is estimated to be within 1 percent. It was expected, and verified by preliminary calculations, that the results would tend to be more inaccurate toward the extremities of the airfoil than near the center. This result is evident from equation (17). A given inaccuracy in the slopes $d\Delta x/d\varphi$ and $d\Delta y/d\varphi$ can produce a large error in the velocity near the extremities, where $\sin \varphi$ approaches zero. This disadvantage does not appear in the Theodorsen-Garrick method, in which $\sin \varphi$ is replaced by one. Excessive error in these regions can be avoided in various ways.

If the initial airfoil, for which the slopes $d\Delta x_0/d\varphi$ and $d\Delta y_0/d\varphi$ have presumably been computed accurately, is a good approximation in these regions, as evidenced by the smallness of δx_1, δy_1 compared to Δx_0, Δy_0, the effect of inaccuracy of the slopes $d\delta x_1/d\varphi$, $d\delta y_1/d\varphi$ will be reduced, since they are added to the initial slopes $d\Delta x_0/d\varphi$, $d\Delta y_0/d\varphi$. It was to reduce the magnitude of the incremental CMF near the leading edge that the NACA 6512 airfoil was drawn tangent to the initial airfoil in this region.

The error in the derivatives can also be avoided by computing them from the differentiated Fourier series for δx_1, δy_1. (See appendix A.) This calculation was made in the illustrative example, after it was found that an error of about 5 percent in the velocity on the upper surface leading edge could be caused by unavoidable inaccuracy in measuring the incremental slopes.

The fact that the computed derivatives do not represent the derivatives of the CMF but rather the derivative of its Fourier expansion to a finite number of terms may introduce inaccuracy. (The derivative Fourier series converges more slowly than the original series.) A comparison of the computed derivatives with the measured slopes will indicate the limits of error, however, as well as the true derivative curve.

The importance of knowing the CMF derivatives accurately may make it desirable to solve the direct problem from the airfoil slopes, rather than from the airfoil itself, as given data. This variation of technique enables the CMF derivatives rather than the CMF itself to be approximated initially. Further details are given in reference 1.

II - THE INVERSE POTENTIAL PROBLEM OF AIRFOIL THEORY

The inverse potential problem of airfoil theory may be stated as follows: Given the velocity distribution as a function of percent chord or surface arc of an unknown airfoil - to derive the airfoil. Before the questions of existence and uniqueness of a solution to the problem as thus stated are discussed, several CMF methods of solution will be outlined and illustrated by numerical examples. Various previous methods of solution will then be described briefly and their inherent limitations and restrictions on the prescribed velocity distribution will be compared with those of the CMF methods.

The prescribed velocity distribution is assumed to be either a double-valued continuous function of the percent chord or a single-valued continuous function of percent arc. (Isolated discontinuities in velocity are, however, at least in the percent-chord case, admissible.)

CMF Method of Potentials

This inverse method is based on the fact that, if the airfoil and its corresponding flat plate and circle are immersed in the same free-stream flows and have the same circulation, conformally corresponding points in the three planes have the same potential.

Consider first the case where a velocity distribution corresponding to a symmetrical airfoil at zero lift is specified as a function of percent chord. If an initial airfoil is assumed, the prescribed velocity can be integrated along its surface to yield an approximate potential distribution as a function of percent chord. This potential increases from zero at the leading edge to a maximum value at the trailing edge. Of fundamental importance to the success of the method is the fact that this potential curve depends mainly on the prescribed velocity distribution and only to a much lesser extent on the form of the initially assumed airfoil. The chord line of the initial airfoil taken as the x-axis is next sufficiently extended that, in the same free-stream flow as for the airfoil, the potential, which in this case is simply $V\xi$, increases linearly from zero at its leading edge to the same maximum value at the trailing edge as exists for the approximate potential curve derived initially. Horizontal displacements Δx between these curves are then measured as a function of the straight-line abscissas and, hence, as a function of the central angle φ of the circle corresponding to the straight line. These horizontal displacements $\Delta x(\varphi)$, together with the conjugate function $\Delta y(\varphi)$ computed therefrom and the length of straight line previously determined, constitute a CMF for an airfoil that is a first approximation to the unknown airfoil. The approximation is based on the use of a more or less arbitrary initial airfoil to set up the first approximate potential. The exact velocity distribution of the derived first approximate airfoil can now be computed and compared with the prescribed velocity. If the agreement is not satisfactorily close, the procedure is repeated, with the airfoil just derived taking the place of the one initially assumed.

The complication introduced in the general case in which the prescribed velocity distribution corresponds to an unsymmetrical airfoil with circulation can be resolved as follows: It is convenient in this case to discuss the potentials in the circle plane. The prescribed velocity distribution is transferred to the circle plane by means of the stretching factor, presumed known, of the initially assumed airfoil; that is, equation (14) is solved for $v_p(\varphi)$. The first approximate potential distribution as a function of the central angle φ is obtained by integrating $v_p(\varphi)$ through a φ-range of 2π radians (around the airfoil), starting from the value of φ near zero for which $v_p(\varphi)$ is zero (the front stagnation point). This approximate potential curve has a minimum value of zero at the front stagnation point, rises to a maximum for the value of φ near π corresponding to the rear stagnation point, then falls to a minimum for the final value of φ (the front stagnation point), which is an angle 2π radians from the starting φ-point. The difference between the final and the initial potential minimums is a first approximation to the circulation Γ.

A circle of such diameter is now derived which, with this circulation and the same free-stream flow as for the airfoil, yields a potential distribution (henceforth called true potential distribution) that has the same maximum and minimum values as the approximate potential curve just derived. If the maximum approximate potential is denoted by r_oU and the decrease of potential (considered positive) from the maximum to the final value by r_oL, where r_o is the diameter of the circle corresponding to the initial airfoil, the parameter γ is first computed from

$$\frac{\pi}{2(\gamma + \cot \gamma)} = \frac{U - L}{U + L} \tag{28}$$

by means of figure 8. The desired diameter r is then given by

$$r = \frac{r_o(U + L)}{4(\cos\gamma + \gamma\sin\gamma)} \tag{29}$$

The parameter γ is actually the sum of the angle of attack and zero-lift angle of the unknown airfoil, to a first approximation; that is,

$$\gamma = \alpha + \beta_T \tag{30}$$

It is related to the circulation Γ by equation (18).

This procedure for the calculation of the diameter (see, for example, reference 6) follows easily from the expression for the potential distribution on a circle, obtained by integration of equation (15) as

$$\Phi_t(\varphi) = r_o\int_{-\beta_N}^{\varphi} v_p(\varphi)d\varphi$$

$$= r_o\left[\cos\gamma + \gamma\sin\gamma - \cos(\varphi + \alpha) + (\varphi + \alpha)\sin\gamma\right] \tag{31}$$

If the diameter r of the derived circle is much greater than the diameter r_o of the circle corresponding to the initial airfoil, it is desirable to increase the CMF Δx_o, Δy_o of the initial airfoil by a factor sufficient to modify the initial airfoil such that it corresponds to a circle of diameter r. A new approximate and true potential distribution is then obtained as described but by using the modified initial airfoil.

The first approximate horizontal displacement function is now determined as the sum of the horizontal displacement $\Delta x_o(\varphi)$ corresponding to the (modified) initial airfoil and an increment $\delta x_1(\varphi)$ produced by the noncoincidence of the approximate potential distribution Φ_a and the true potential distribution Φ_t. This horizontal increment may be measured between the two potential curves, both considered plotted against chordwise position in the physical plane. With sufficient accuracy this increment may be computed as the vertical distance between the potential curves divided by the slope of the approximate potential curve; namely, the prescribed velocity v_z. If, therefore, all quantities are considered as functions of φ

$$\begin{aligned}\Delta x_1 &= \Delta x_o + \delta x_1 \\ &= \Delta x_o + \frac{\Phi_a(\varphi) - \Phi_t(\varphi)}{v_z(\varphi)}\end{aligned} \tag{32}$$

The ordinate function $\Delta y_1(\varphi)$ conjugate to $\Delta x_1(\varphi)$ can now be computed and, together with $\Delta x_1(\varphi)$ and the diameter r obtained previously, determines the first approximate airfoil by equations (9) and (10). Calculation or measurement of the CMF derivatives $d\Delta x_1/d\varphi$, $d\Delta y_1/d\varphi$ and the use of equations (11) and (17) then determine the zero lift angle β_T and the exact velocity distribution of the first approximate airfoil. The angle of attack, to a first approximation, is given by equation (30), the value of γ derived from equation (28) being used. This exact velocity distribution is compared with that prescribed and, if the agreement is not close enough, the procedure can be repeated with the first approximate airfoil as the initial airfoil.

In the case where the prescribed velocity is specified as a function of percent arc, then by line integration of the prescribed velocity along the percent arc, the true potential distribution of the unknown airfoil is known as a function of arc (except for a trivial scale factor). The maximum and minimum values of this potential distribution then permit the unique determination, by the calculation previously described, of the circle corresponding conformally to the unknown airfoil. Correlation of the potential distribution of this circle with the potential distribution as a function of arc initially calculated therefore yields exactly the potential distribution of the unknown airfoil as a function of the central angle φ of the circle. This fact has been noted by Gebelein (reference 6). The calculation of the diameter r as outlined above for the percent-chord case is thus unnecessary. The remainder of the procedure is the same, the successive approximate airfoils now being adjusted to correspond conformally to this circle. before correlating their percent-arc lengths with the prescribed velocity distribution in preparation for the next approximation.

The successive contours determined by the method of potentials are, of necessity, closed contours, whether or not the sequence of contours converges to a solution satisfying (mathematically) the prescribed velocity distribution. The closure of the contours is a consequence of the method of setting up the horizontal displacements, $\Delta x(\varphi)$, and solving for $\Delta y(\varphi)$, by which the contour coordinates are obtained as single-valued functions of φ. The necessity for closed contours does not, however, exclude the possibility of deriving physically unreal shapes; namely, contours of figure-eight type. This point will be discussed at greater length later but it may be remarked here that it is the extra degree of freedom introduced by the class of figure-eight type contours that admits the possibility of a unique solution to the inverse problem treated here.

It will have been noticed that, whereas in the direct method a Δy is determined from the given data - that is, the airfoil - and a Δx is computed therefrom, conversely, in the inverse method of potentials a Δx is determined from the given data - that is, the velocity distribution - and a Δy is computed therefrom. Similarly, just as the direct problem can also be solved by deriving $d\Delta y/d\varphi$ from the given airfoil slopes and thence computing $d\Delta x/d\varphi$, so, conversely, can the inverse problem be solved by deriving $d\Delta x/d\varphi$ from the prescribed velocity distribution and thence computing $d\Delta y/d\varphi$. This inverse method of derivatives will be discussed after some numerical examples are presented, illustrating the method of potentials.

Examples of CMF Method of Potentials

Symmetrical section.- The method of potentials was applied first to the derivation of the symmetrical profile corresponding to the prescribed velocity distribution shown in figure 9(a). As an initial airfoil the 12-percent thick profile derived from the 30-percent thick Joukowski profile in part I was used. The initial CMF and associated constants are given in table VII. The initial airfoil and its velocity distribution are shown in figure 9. The first increment CMF and the resultant first approximate airfoil and its exact velocity distribution were calculated by the procedure of the preceding section. The incremental slopes $d\delta x_1/d\varphi$, $d\delta y_1/d\varphi$ were computed and found to approximate the measured slopes very closely. The results are presented in table VII and figure 9. It is seen that the change in velocity and profile accomplished by one step of the inverse process is large; that is, the convergence is rapid. The high velocity of the first point on the upper surface ($\varphi = 15^\circ$) is due to lack of detail in the calculation. (Twelve points on the upper surface were calculated.) For practical purposes the nose could be easily modified to reduce this velocity if desired without going through a complete second approximation.

Mean camber line for uniform velocity increment.- As a second example of the inverse CMF method, the profile producing uniform equal and opposite velocity increments on upper and lower surfaces was derived. By the methods of thin-airfoil theory this velocity distribution yields the so-called logarithmic camber line. The prescribed velocity distribution is indicated in figure 10(a). The velocity peaks at the extremities of the prescribed velocity curve were assumed in order to compensate for an expected rounding off of the velocity in this region in working up from the initial velocity distribution. The convergence to the prescribed uniform velocity distribution would thereby be accelerated. The initial airfoil was taken as the 6-percent camber circular arc, discussed in part I. The initial CMF and its associated constants are given in tables III and IV. The circular arc and its velocity distribution are shown in figure 10.

A first approximation was calculated as outlined in the previous section. A numerical difficulty appeared in the process of solving equation (11) for the zero-lift angle of the first approximate airfoil. It appeared that a 24-point calculation (12 points by symmetry) did not give sufficient detail in the range $\pi < \varphi < \frac{13}{12}\pi$ to yield a reliable solution of equation (11) for the zero-lift angle. This result was a consequence of the prescribed velocity discontinuity at the extremities with the consequent large but local changes in CMF and profile shape required in these regions. The solution obtained for the zero-lift angle was $\beta_T = 6.1^\circ$, which by equation (19) with $r = 1.0043$ and $\alpha_1 = 0$ yielded $c_l = 0.67$. The desired c_l, however, is 0.80, which would correspond to $\beta_T = 7.27^\circ$. It was considered that a relatively minute change in the shape of the extremities of the derived camber line would alter the slope $d\Delta x_1/d\varphi$ in the desired range sufficiently to yield a zero-lift angle of $\beta_T = 7.27^\circ$. On the other hand the effect of such a local change on the CMF as a whole would be small. The velocity distributions of the derived profile were therefore computed for both zero-lift angles quoted previously.

The results are given in table VIII and in figure 10. Included for comparison in figure 10(b) (vertical scale magnified) is the logarithmic mean line of thin-airfoil theory, computed for $c_l = 0.80$. The velocity distribution of the derived shape as calculated for the desired lift coefficient of $c_l = 0.80$ is seen to be a satisfactory approximation to the desired rectangular velocity distribution. The profile itself is seen to be one of finite thickness as compared with the single line of thin-airfoil theory. Airfoils obtained by superposition of this type of camber line with thickness profiles would therefore be increased in thickness over that of the basic thickness form.

The changes in velocity distribution and in shape of profile are again seen to be large; that is, the convergence was rapid. As is to be expected, the rapidity of convergence of both the direct and inverse methods in comparable cases is about the same.

CMF Method of Derivatives

Instead of approximating by the method of potentials to a CMF that, when differentiated, yields the prescribed velocity, the CMF derivatives may be obtained directly. The controlling equations are equations (17), (9), and a modification of equation (7).

$$v_z(\varphi) \doteq \frac{\left|\sin(\varphi + \alpha) + \sin\left(\alpha + \beta_T\right)\right|}{\sqrt{\left(\frac{d\Delta x}{r\ d\varphi} - \sin\varphi\right)^2 + \left(\frac{d\Delta y}{r\ d\varphi}\right)^2}} \tag{17}$$

$$\frac{d\Delta y}{d\varphi} = \frac{1}{2\pi}\int_0^{2\pi} \frac{d\Delta x}{d\varphi'} \cot\frac{\varphi' - \varphi}{2}\, d\varphi' \tag{7a}$$

$$\frac{x}{r} = \cos\,\varphi \;+ \frac{1}{r}\,\Delta x(\varphi) \tag{9}$$

These equations, together with the auxiliary equations (11) and (18), constitute a set of simultaneous equations from which the CMF derivative $d\Delta x/d\varphi$ may be determined from a prescribed velocity distribution v_z. The corresponding airfoil is determined by integration of $d\Delta x/d\varphi$ and its conjugate $d\Delta y/d\varphi$.

Consider first the case where the velocity is specified as a function of percent arc. As explained in the previous section, the constants r and γ of the final circle corresponding to the unknown airfoil can in this case be determined initially. Points of equal potential along the arc and circle are then found, which yield v_z as a function of φ. The angle of attack α in equation (17) is taken as some reasonable value and $d\Delta x/r\,d\varphi$ determined by successive approximation. In the first approximation $d\Delta y/r\,d\varphi$ may, for example, correspond to some known CMF. Equation (17) is then solved for $d\Delta x/r\,d\varphi$, for which the conjugate $d\Delta y/r\,d\varphi$ is calculated next and used as a basis for a better determination of $d\Delta x/r\,d\varphi$. The airfoil corresponding to any approximation is obtained by integration of $d\Delta x/d\varphi$ and its conjugate $d\Delta y/d\varphi$. (The method of derivatives may be regarded as based on the use of the function $ip\,\frac{d(z - \zeta)}{dp}$. This function is regular everywhere outside the circle $p = Re^{i\varphi}$, approaches zero at infinity, and reduces to $\frac{d\Delta x}{d\varphi} + i\,\frac{d\Delta y}{d\varphi}$ on the circle itself.)

In general the $d\Delta x/d\varphi$ as determined in any approximation will have an average value other than zero. The $\Delta x(\varphi)$ obtained, say, by integration of its Fourier series would therefore contain a term proportional to φ in addition to a Fourier series. Thus, $\Delta x(\varphi)$ would not be a single-valued function of φ and the resulting contour would not close. Simply subtracting the average value of $d\Delta x/d\varphi$ (the constant term in its Fourier series), however, will close the derived contour. If the method converges, this average value approaches zero in the successive approximations.

A preliminary over-all adjustment of an initially chosen CMF may be desirable. Thus, if $d\Delta x_1/d\varphi$ is calculated in terms of the $d\Delta y_0/d\varphi$ of a previous approximation and is found to be larger than $d\Delta x_0/d\varphi$ by some factor, $d\Delta y_0/d\varphi$ can be multiplied by this factor and the calculation of $d\Delta x_1/d\varphi$ repeated.

Although the angle of attack may be arbitrarily set initially in this calculation it should be so chosen that the final airfoil will coincide approximately in position with the initial airfoil. After each calculation of $d\Delta x/d\varphi$, the zero-lift angle β_T can be calculated, equation (11), which thereupon fixes α, since $\gamma = \alpha + \beta_T$ is known.

If the prescribed velocity distribution is specified as a function of percent chord, $v_z(\varphi)$ must be determined in the successive approximations by use of equation (9). The quantity $\gamma = \alpha + \beta_T$ may be determined in each approximation as in the method of potentials or, in physically real cases, by equation (19). The diameter r is so determined that the successive airfoils are of a standard chord length.

It is evident from the structure of equation (17) that near the airfoil extremities where $\sin\varphi \longrightarrow 0$, and in particular at the nose of the airfoil where $d\Delta y/d\varphi$ is comparable to $d\Delta x/d\varphi$ in magnitude, the convergence by this method (and by the method of potentials) will be comparatively slow. If modifications to the airfoil only in the immediate neighborhood of the nose are required, it may be more expedient to apply a preliminary Joukowski transformation, that is, to use these methods with the Theodorsen-Garrick transformation.

An example of the use of the CMF method of derivatives to solve an inverse problem is given in reference 1 for the case of a cascade of airfoils.

Method of Betz

In the inverse method of Betz (reference 7) an airfoil and its velocity distribution are assumed known (fig. 11) and a desired velocity is specified as a function of percent arc. The new velocity and length of arc are specified in such a way that the extremities of potential are the same as on the known airfoil. Both known and unknown airfoils then transform into the same circle and, in particular, the velocities at points of equal potential on the two profiles can be found.

In order to determine the profile corresponding to the new velocity, the complex displacement $z_2 - z_1$ between points of equal potential on the two profiles is expressed as a function of the corresponding complex velocities (denoted by v_z) thus,

$$\frac{d}{dz_1}\left(z_2 - z_1\right) = \frac{dz_2}{dz_1} - 1 = \frac{dw/dz_1}{dw/dz_2} - 1 = \frac{v_{z_1}}{v_{z_2}} - 1$$

Hence

$$z_2 - z_1 = \int_T^{z_1}\left(\frac{v_{z_1}}{v_{z_2}} - 1\right) dz_1 \tag{33}$$

where the integration is carried out along the known profile from the trailing edge, which is taken as coincident for the two airfoils, to the point z_1. The complex function v_{z_1}/v_{z_2} is determined approximately from the known ratio $\left|\frac{v_{z_1}}{v_{z_2}}\right|$ corresponding to the points of equal potential by the argument that, inasmuch as the two profiles have nearly the same slope at corresponding points, the real part of $\frac{v_{z_1}}{v_{z_2}} - 1$ is given by $\left|\frac{v_{z_1}}{v_{z_2}}\right| - 1$. (This assumption, like the approximations in the CMF methods, is least valid at the nose of the airfoil. The function $z_2 - z_1$ is in fact a Cartesian mapping function.) The imaginary part is then computed as the conjugate function, equation (7).

In addition to the restrictions on the velocity distribution mentioned initially, further conditions must be met in this method, if closed contours are to be obtained. Thus, the condition for closure of contour,

$$\int_C d\left(z_2 - z_1\right) = \int_C\left(\frac{v_{z_1}}{v_{z_2}} - 1\right) dz_1 = 0 \tag{34}$$

and the required coincidence of v_{z_2} and v_{z_1} at infinity, lead to the following three restrictions on the real part $R(\varphi)$ of the integrand in equation (34) considered as a function of φ in the circle plane,

$$\int_0^{2\pi} R(\varphi)d\varphi = \int_0^{2\pi} R(\varphi)\cos\varphi\, d\varphi = \int_0^{2\pi} R(\varphi)\sin\varphi\, d\varphi = 0 \qquad (35)$$

Method of Weinig and Gebelein

The method of Weinig and Gebelein (reference 6) may be described essentially as follows: The given data are the same as in the Betz method. Consider the function

$$\log\frac{v_{z_2}}{v_{z_1}} = \log\left|\frac{v_{z_2}}{v_{z_1}}\right| - i\left(\beta_{z_2} - \beta_{z_1}\right) \qquad (36)$$

where β_{z_2} and β_{z_1} are the slopes at corresponding points of the two airfoils (fig. 11). Since $|v_{z_2}|$ and $|v_{z_1}|$ are known functions of φ with the data as given, and since $\log\frac{v_{z_2}}{v_{z_1}}$ is regular outside the circle, $\beta_{z_2} - \beta_{z_1}$ can be calculated as the function conjugate to $\log\left|\frac{v_{z_2}}{v_{z_1}}\right|$. The angle β_{z_1} being known, β_{z_2} is thereby determined and hence, by simple integration, the unknown airfoil coordinates are obtained.

As in the Betz method, the condition for closure of the desired contour

$$\int_C dz = \int_C \frac{dw/dp}{dw/dz}\, dp = \int_C \frac{v_p}{v_z}\, dp = 0 \qquad (37)$$

leads to the additional restrictions on the prescribed velocity distribution,

$$
\left.
\begin{aligned}
\frac{1}{2\pi}\int_0^{2\pi} \log\left|v_z(\varphi)\right| d\varphi &= 0 \\
\frac{1}{\pi}\int_0^{2\pi} \log\left|v_z(\varphi)\right| \sin\varphi \, d\varphi &= -\sin 2\gamma \\
\frac{1}{\pi}\int_0^{2\pi} \log\left|v_z(\varphi)\right| \cos\varphi \, d\varphi &= -\pi(1 - \cos 2\gamma)
\end{aligned}
\right\} \qquad (38)
$$

where γ is given by equation (30).

Discussion of the Various Inverse Methods

The methods of Betz and of Weinig-Gebelein may be somewhat narrower in scope than the CMF methods. The use of mapping functions such as in equations (33) and (36) is based on the ability to specify dz_2/dz_1 unambiguously in the corresponding regions. This requirement appears to restrict the contours obtainable by these methods to those bounding simply connected regions. Further investigation of this point is necessary, however. By the CMF methods, figure-eight contours have arisen in the course of solution of both the direct and the inverse problems. (See the 9-percent camber derived mean line (fig. 5(a)) and the illustrative examples in reference 1.) Such contours were first encountered as preliminary results (unpublished) in using the method of potentials with the Theodorsen-Garrick transformation. The CMF apparently makes no fundamental mathematical distinction between simply connected and figure-eight contours, for although $z - \zeta$ must be a single-valued function of z, ζ, or p, the coordinate z itself is of the same character as ζ and the latter has two Riemann sheets at its disposal in consequence of the Joukowski transformation from the ζ- to the p-plane.

The methods of Betz and of Weinig-Gebelein require the numerically difficult closure conditions (equations (35) and (38)) to be satisfied in advance. If the methods are worked through for prescribed velocity distributions which do not satisfy these conditions, it appears that open contours result. In the CMF methods, however, there is either no closure condition (method of potentials) or a numerically simple one (method of derivatives):

$$\int_0^{2\pi} \frac{d\Delta x}{d\varphi}\, d\varphi = \int_0^{2\pi} \frac{d\Delta y}{d\varphi}\, d\varphi = 0$$

[This simple closure condition in the method of derivatives is fundamentally a consequence of the fact that the required absence of the constant term in the inverse power series for the CMF derivative mapping function $\left(ip\,\frac{d(z - \zeta)}{dp},\right.$ mentioned previously$\left.\right)$ automatically excludes the inverse first power (the residue term) from the power series for $d(z - \zeta)/dp$.] Thus, physically impossible velocity distributions lead to open contours in the Betz-Weinig-Gebelein methods and to figure-eight contours in the CMF methods (if the latter converge). From the practical point of view in these cases, it may be easier to obtain the airfoil corresponding to the "best possible" physically attainable velocity distribution by the CMF methods than by the others. If the succession of airfoils determined by an inverse CMF method is seen to tend toward the development of a figure-eight, the successive approximations can be stopped at the "best possible" physically real airfoil.

As to the existence and uniqueness of a solution to the inverse problem as stated, a rigorous discussion of the solutions, for a prescribed velocity distribution, of the controlling equations (17), (7a), and (9) is lacking. For physically possible velocity distributions, however, specified as a function of percent arc, the Weinig-Gebelein method shows that there is one and only one airfoil as a solution. If, however, the velocity is specified as a function of percent chord, some further condition is necessary. This requirement is evident from the fact that one velocity distribution for an airfoil can, for differently chosen chords, be expressed as a different function of percent chord in each case. One chord with a given velocity as a function of percent chord can therefore have more than one corresponding airfoil. There is reason to suppose that the further condition for uniqueness of solution in this case is, the chord being defined as in the section "The Direct Potential Problem for Airfoils," that the ordinates to the airfoil at the chordwise extremities be specified.

From the experience with the CMF methods gained to date, it is believed that to a velocity distribution specified as at the beginning of part II, and with the further condition mentioned in the percent-chord case, there corresponds one and only one closed contour satisfying the CMF system of equations. It is furthermore believed that the CMF methods are flexible enough to converge to this solution in at least those cases of aerodynamic interest.

CONCLUSIONS

1. The conformal transformation of an airfoil to a straight line by the Cartesian mapping function (CMF) method results in simpler numerical solutions of the direct and inverse potential problems for airfoils than have been hitherto available.

2. The use of superposition with the CMF method for airfoils provides a rigorous counterpart of the approximate methods of thin-airfoil theory.

Langley Memorial Aeronautical Laboratory
National Advisory Committee for Aeronautics
Langley Field, Va.

APPENDIX A

THE CALCULATION OF CONJUGATE FUNCTIONS

BY THE RUNGE SCHEDULE

The basic calculation for the type of mapping function treated in this paper and in reference 2 consists of the computation of the real part of an analytic function on a circle, given the imaginary part, or vice versa. To this end the conjugate Fourier series, equations (4) and (5), or the conjugate integral relations, equations (6) and (7), are available. This type of calculation appears to be fundamental in many kinds of two-dimensional potential problems. For example, the solution of the integral equation relating normal induced velocity to circulation in lifting-line theory can be solved easily by a method of successive approximation if the transformation from the "lifting line" to the circle is known. Quicker methods of calculating a function from its conjugate than those given in this appendix or in reference 2 would therefore be highly useful.

The use of the Fourier series rather than the integral relations in the calculations of this paper was based on the following consideration. Because the function $1/z$ is regular outside the unit circle, the real and imaginary parts of $1/z$ on the unit circle, namely, $\cos \varphi$ and $-\sin \varphi$, satisfy the integral relations (6), (7). The substitution of $-\sin \varphi$ for Δy in equation (6) and subsequent numerical evaluation by the 20-point method of reference 2 gave results that were higher than $\cos \varphi$ by a constant error of 2.8 percent. Evaluation by a 40-point method reduced the error by half, or to 1.4 percent. By the Fourier series, on the other hand, the first harmonic (a one-point method) suffices to give exact results in this case. It appears, therefore, that when the given real function is expressible in terms of a small number of harmonics, as is the case in airfoil applications, the Fourier series method is preferable to the use of the integral relations.

The Runge schedule offers a convenient means of carrying out the basic calculation of mapping functions, namely, the analysis of a periodic function into its

Fourier series and the synthesis of a Fourier series into a function. The theory and use of the schedule is described, for example, in reference 8, wherein are also given schedules for 12-, 24-, 36-, and 72-point harmonic analyses.

The necessary analyses and syntheses in the direct and inverse CMF methods are carried out in accordance with equations (4) and (5) and their derivatives. Table IX contains the scheme of substitution into the Runge schedule, table X, for the various CMF methods. In the direct method, for example, the set of values $\delta y/12$ corresponding to the evenly spaced φ-values is substituted into the y_n spaces at the beginning of the sum-table. The sums and differences of these quantities are then obtained as directed at the left of the individual tables and substituted into the succeeding tables. In this way the entire sum-table is filled out. Before the product-table is used, the sum-table should be checked.

The quantities surrounded by the heavy lines in the sum-table are next multiplied by the proper factors at the left of the product-table and the results entered in the appropriate spaces as indicated by the letters at the left of the individual product-spaces. A heavy horizontal line at the lower left edge of a product-space indicates that the corresponding product has already been obtained in a previous space in the same row. A heavy vertical line along the left edge of a product-space is used to emphasize that the negative value of the product of the sum-table quantity and the product-table factor is to be entered. The sums of the product-table columns are then entered in the I, II, III, and IV spaces. A check on the work of the product-table up to this point is provided by the columns at the right. The sums and differences of the I, II, III, and IV quantities complete the product-table and give the Fourier coefficients a_n, b_n corresponding to δy.

In order to perform a synthesis calculation from a set of Fourier coefficients a_n, b_n to the values of the corresponding function at the even φ-points, the coefficients a_n, b_n are entered in the d and D spaces, respectively, in the sum-table, and the remainder of the sum-table and the product-table worked through as before. The final values in the a_n, b_n spaces of the product-table are then entered in the d and D spaces at the beginning of the sum-table and the sums and differences obtained as indicated by the synthesis column at the left. (Note that d_0 and d_{12} are to be multiplied by 2.) The resulting y_n quantities are the desired values of the function.

The numerical values in tables X(a) and (b) illustrate the process of obtaining $\delta x_1(\varphi)$ from $\delta y_1(\varphi)$ in the first approximation by the direct CMF method for the NACA 6512 airfoil.

APPENDIX B

THE MAPPING OF MORE GENERAL REGIONS

Simply Connected Regions

If the CMF method is applied to the mapping of a simply connected boundary with a vertical discontinuity, such as a rectangle or an infinite line with a vertical step, the ambiguity of the ordinate Δy at the discontinuity will prevent an automatic and rapid convergence of the method. Although the difficulty could be lessened in particular cases such as for rectangles by taking the diagonal as x-axis, thus removing the vertical discontinuity, or by using symmetry, as with squares, it is evident that in general a reference shape particularly suited to the contour under investigation is needed. The circle has been shown in reference 2 to be a good reference shape for the square. It could be expected therefore that an ellipse would be a good reference shape for the rectangle. Furthermore, just as the mapping function based on the circle was formed of an angular displacement and a radial displacement, the mapping function based on the ellipse should be formed of displacements along and orthogonal to the ellipse, that is, should be specified by elliptic coordinates. The specification of a figure by elliptic coordinates (ψ, θ) in the physical plane z is equivalent, however, to the transformation of the figure to a t'-plane by the two transformations

$$\left.\begin{aligned} z &= p' + \frac{1}{p'} \quad \text{where} \quad p' = e^{\psi+i\theta} \\ t' &= \log p' \quad \text{where} \quad t' = \psi + i\theta \end{aligned}\right\} \tag{39}$$

and specifying the transformed figure by the Cartesian coordinates of the t'-plane (ψ, θ). The rectangle under consideration will be a near-circular shape in the p'-plane and a near-straight line shape in the t'-plane. The mapping of the rectangle by means of an elliptic mapping function in the physical plane is therefore seen to be accomplished by the Theodorsen-Garrick method in the near-circle p'-plane and by the CMF method in the near-straight line t'-plane. From this point of view, therefore, the Theodorsen-Garrick method consists of specifying an airfoil in the physical plane by elliptic coordinates, forming the corresponding elliptic mapping function $(\psi - \psi_o) - i\epsilon$, which conformally relates the airfoil to an ellipse or Joukowski airfoil as a basic shape, and expressing the elliptic mapping function as a regular function outside the circle. On the other hand, in the $t' = \log\ p'$-plane the Theodorsen-Garrick method consists of the transformation of the near-straight line $\psi(\theta)$ to the straight line ψ_o = Constant by means of what is now the CMF $(\psi - \psi_o) - i\epsilon$. Thus, the Theodorsen-Garrick method may be regarded as a form of the CMF method, in which $\log p'$ takes the place of z and $\log p$, the place of ζ.

The mapping of simply connected regions by difference mapping functions based on the curvilinear coordinates appropriate to the particular reference shape considered is therefore equivalent to using the CMF difference function $z - \zeta$ in the plane of the near-straight line into which the reference shape is initially transformed.

Mapping of the Entire Field

The Fourier series representation of mapping functions, equations (4) and (5), enables the calculation of corresponding points in the two regions to be made, once the correspondence of the boundaries has been calculated. By the latter calculation the coefficients a_n, b_n and the radius R of the circle of correspondence have been determined. If now a larger radius $R' > R$ be substituted for R in equations (4) and (5), the resulting synthesis of the Fourier series will yield the mapping function for the circle of radius R'; that is, will determine points in the given plane corresponding to the points in the circle plane at the distance R' from the origin. It is necessary, of course, to use the mapping function in conjunction with the shape in the physical plane corresponding to the larger circle. In this way the entire corresponding fields can be mapped out. It may be noted that substitution of $R' < R$ for R in equations (4) and (5) enables the mapping of those corresponding points inside the original contours for which the resulting Fourier series converge.

It appears to be more difficult to find the point in the circle plane corresponding to a point of the given plane than vice versa. This calculation may, however, be accomplished by a method of successive approximations. For example, if the given plane is that of a near circle the polar coordinates of the given point in the near-circle plane are assumed to be a first approximation to the coordinates R' and φ of the desired point in the circle plane. Substitution of these values into equations (4) and (5) yields a first approximate mapping function which can be used to correct the coordinates R' and φ, etc.

Biplanes

In the case of the biplane arrangement the CMF may be set up directly in the physical plane in the same way as for the single airfoil. In place of the simple transformation from straight line to circle, however, the transformation from the two extended chord lines of the airfoils to two concentric circles is used. This transformation is derived in reference 9. The CMF method for biplanes bears the same relation to the method of reference 9 that the CMF method for monoplane airfoils bears to the Theodorsen-Garrick method (reference 2).

For biplanes (fig. 12) the CMF $z - \zeta$, being regular in the region outside the two straight lines, is regular in the annular region of the p-plane and consequently is expressible as a Laurent series in p

$$\left.\begin{aligned} z - \zeta &= \sum_{-\infty}^{\infty} \frac{c_n}{p^n} \\ \text{where} \qquad & \\ c_n &= a_n + ib_n \end{aligned}\right\} \qquad (40)$$

If, for the inner circle, the relationship is written

$$\left.\begin{aligned} z - \zeta &= \Delta x_1 + i\,\Delta y_1 \\ p &= R_1 e^{i\varphi} \end{aligned}\right\} \qquad (41)$$

and for the outer circle

$$\left.\begin{aligned} z - \zeta &= \Delta x_2 + i\,\Delta y_2 \\ p &= R_2 e^{i\varphi} \end{aligned}\right\} \tag{42}$$

there is obtained, upon substitution into equation (40) and reduction

$$\Delta x_1(\varphi) = a_o + \sum_1^\infty \frac{a_n + a_{-n}}{R_1{}^n} \cos n\varphi + \sum_1^\infty \frac{b_n - b_{-n}}{R_1{}^n} \sin n\varphi \tag{43a}$$

$$\Delta x_2(\varphi) = a_o + \sum_1^\infty \frac{a_n + a_{-n}}{R_2{}^n} \cos n\varphi + \sum_1^\infty \frac{b_n - b_{-n}}{R_2{}^n} \sin n\varphi \tag{43b}$$

$$\Delta y_1(\varphi) = b_o + \sum_1^\infty \frac{b_n + b_{-n}}{R_1{}^n} \cos n\varphi - \sum_1^\infty \frac{a_n - a_{-n}}{R_1{}^n} \sin n\varphi \tag{43c}$$

$$\Delta y_2(\varphi) = b_o + \sum_1^\infty \frac{b_n + b_{-n}}{R_2{}^n} \cos n\varphi - \sum_1^\infty \frac{a_n - a_{-n}}{R_2{}^n} \sin n\varphi \tag{43d}$$

Those equations are the generalization to the biplane of equations (4) and (5). The corresponding integral relations may be derived as in reference 9.

The solution of equations (43) in either the direct or the inverse problem may be accomplished as before by successive approximations. For example, in the direct method the two airfoils are given. If no initial approximation biplane were available, the two chord lines would be taken as the initial straight lines. By the transformation of reference 9 this fixes the chordwise locations on the straight lines corresponding to a set of evenly spaced φ points on the concentric circles. The ordinates $\Delta y_1(\varphi)$ can therefore be measured, which determines $\Delta y_2(\varphi)$ by analysis and synthesis of equations (43c) and (43d), respectively. (The radius ratio R_2/R_1 is fixed by the initial transformation from the straight lines to the concentric circles.) These $\Delta y_2(\varphi)$ values then determine a set of $\Delta x_2(\varphi)$ values by the given shape of the second airfoil and the known chordwise locations of its first approximation straight line. Analysis of $\Delta x_2(\varphi)$ and subsequent synthesis of $\Delta x_1(\varphi)$ by equations (43b) and (43a), respectively, determines a correction to R_1 by a horizontal stretching process (constant Δx, Δy - adjustment of r_1) to maintain the given airfoil chord. The procedure is now repeated with $\Delta y_2(\varphi)$ as the initial set of measured ordinates that determines $\Delta y_1(\varphi)$, $\Delta x_1(\varphi)$, and $\Delta x_2(\varphi)$ as before. The radius R_2 can now be similarly corrected. This step completes the first approximation. For the second approximation a new correspondence between the corrected straight lines and the concentric circles is calculated and the procedure repeated.

The inverse problem could also be solved by methods similar to those given for the isolated airfoil. Suppose, for example, a wing section were given and it were desired to derive a slat of given chord and given approximate location and having a prescribed velocity distribution. The method of surface potentials, for example, enables the calculation of a first approximate $\Delta x_1(\varphi)$ (subscript 1 refers to slat). The initial correspondence of points between the straight lines and concentric circles, and therefore also R_2/R_1, being determined by the initially assumed straight lines, the function $\Delta x_2(\varphi)$ is thereupon obtained by analysis and synthesis of equations (43a) and (43b), respectively. The horizontal displacement $\Delta x_2(\varphi)$ thence determines $\Delta y_2(\varphi)$ by the known shape of the main wing section. The determination of $\Delta y_1(\varphi)$ by analysis and synthesis of equations (43d) and (43c) completes the calculation of the first approximate slat section, for which the exact velocity distribution can now also be calculated. If the main wing section were also unknown then the wing section above is regarded as an initial approximation, the role of the two airfoils is reversed, and the procedure repeated to complete the first approximation.

The CMF method can be generalized in the same manner for multiply connected regions. The transformation from the n reference shapes (such as straight lines) to n circles being presumed known, the CMF can be set up as a series convergent in the region between the n circles, and the mapping function for each boundary explicitly expressed by allowing the coordinate vector to assume its value on each boundary in turn. A method of successive approximation for the solution of the resulting equations depending on the particular problem under consideration would then be established.

Cascade of Airfoils

A simplified but practically important n-body problem, namely, the cascade of airfoils, may be mentioned finally.

The reference shape into which the cascade of airfoils, figure 13, is to be transformed is chosen as the cascade of stright lines coinciding with the extended chord lines of the airfoils of the cascade. The transformation from the cascade of straight lines to a single circle is well-known, reference 10. The CMF chosen as indicated in figure 13 is therefore expressible as an inverse power series in the circle plane and the resulting procedure in either the direct or the inverse problem is seen to be essentially the same as for isolated airfoils. The detailed application of the CMF to cascades of airfoils is given in reference 1.

APPENDIX C

THE DETERMINATION OF MAPPING FUNCTIONS BY THE CAUCHY INTEGRAL FORMULA

The foregoing methods of conformal transformation have been presented from the point of view of representation of the various mapping functions as infinite series. In particular, the expression of the Cartesian mapping function as an inverse power series valid everywhere outside and on a circle led to the Fourier series representation for the CMF on the circle itself. The integral formula representation was then obtained from the Fourier series by the method of reference 3. It is of interest to see how the integral relations (6) and (7) can be derived directly from the Cauchy integral formula for a function regular outside a circle. (These integral relations have also been derived by Betz, reference 7, by a hydrodynamical argument.) Since the applicability of the Cauchy integral formula is not restricted to circular boundaries, however, the results will be capable of generalization, in principle at least, to arbitrary simply and multiply connected regions.

The Cauchy integral formula gives the values of an analytic function $f(p)$ within a simply connected domain D in terms of its values $f(t)$ on the boundary of the domain as

$$f(p) = \frac{1}{2\pi i}\int \frac{f(t)}{t - p}\, dt \tag{44}$$

where the path of integration is counterclockwise around the boundary. Consider the domain D outside the simple closed boundary C in the p-plane (fig. 14). This domain can be made simply connected by an outer boundary B and the cuts between the two boundaries, as indicated by the dotted lines. The Cauchy integral formula for the function $f(p)$ at an interior point p of the domain D, in terms of its values on the boundary is

$$f(p) = \frac{1}{2\pi i}\int_C \frac{f(t)}{t - p}\, dt + \frac{1}{2\pi i}\int_B \frac{f(t)}{t - p}\, dt \tag{45}$$

where the equal and opposite integrals along the cuts have been omitted. The paths of integration are indicated by the arrows in figure 14. The function $f(p)$ is assumed to be regular everywhere outside the boundary C and in particular to approach the limiting value f_∞ as $p \longrightarrow \infty$. If the boundary B is enlarged indefinitely, the integrand of the second integral of equation (45) approaches f_∞/t and thus

$$\lim_{t \longrightarrow \infty} \frac{1}{2\pi i} \int_B \frac{f(t)}{t - p} \, dt = f_\infty \tag{46}$$

The variable p will now be made to approach a point t' on the boundary C, and equation (45) will consequently reduce to an integral equation for the boundary values of a function regular everywhere outside and on the boundary. In order to evaluate properly the contribution of the remaining (first) integral of equation (45) in the neighborhood of t', the boundary C is modified as indicated in figure 14. The point p is made the center of a semicircle whose ends are faired into the original boundary. As $p \longrightarrow t'$, the modified boundary approaches coincidence with the original boundary. The integral over the modified boundary is now evaluated as the sum of the integral over the semicircle, which in the limit is half the residue of the integrand or $\frac{1}{2} f(t')$, and the integral over the rest of the path, which in the limit is analogous to the Cauchy principal value of a real definite integral of which the integrand becomes infinite at some point in the interval of integration. Equation (45) therefore becomes, in the limit,

$$\frac{f(t')}{2} = \frac{1}{2\pi i} \int_C \frac{f(t)}{t - t'} \, dt + f_\infty \tag{47}$$

In addition, there is the auxiliary condition that

$$-\frac{1}{2\pi i} \int_C \frac{f(t)}{t} \, dt = f_\infty \tag{48}$$

which follows from the fact that $f(p)$ is regular everywhere outside the boundary C. Equation (47) is well known in the theory of functions of a complex variable. (See reference 11.)

If, now, the function $f(p)$ is taken as the Cartesian mapping function $z - \zeta$ or, on the boundary,

$$f(t) = \Delta x + i \, \Delta y \tag{49}$$

and if, further, the boundary C is taken as a circle with origin at the center,

$$\left.\begin{aligned} t &= e^{\psi_0 + i\varphi} \\ t' &= e^{\psi_0 + i\varphi'} \end{aligned}\right\} \tag{50}$$

substitution of equations (49) and (50) into equation (47) and using equation (48) (with $f_\infty = 0$) leads to the integral relations (6) and (7). If the polar mapping function $\log \frac{p'}{p} = \Psi - i\epsilon \equiv (\psi - \psi_0) - i(\varphi - \theta)$ (reference 2) is substituted for $f(t)$, the Theodorsen-Garrick integral relations are obtained.

The Cauchy integral formula has already been applied (reference 12) to problems of conformal mapping in the manner just indicated. Bergman has included in reference 12 (chapter XI) contributions of two Russian authors, Gershgorin and Krylov. In reference 12 the mapping function from a circle to a near circle was taken in the form $\log p$. The resulting integral equation does not appear to be as convenient as those of the CMF methods. The use of forms such as $\log \frac{p'}{p}$ or $z - \zeta$ are not only accurate numerically since they express changes in the coordinates of the boundaries, but also they lead to pairs of integral equations which contain the solutions of both the direct and the inverse potential problems.

From the analysis given it appears possible to transform conformally from one boundary to another without requiring the transformation from either boundary to a circle, since the boundary C in equation (47) can be rather arbitrary and $f(t)$ can be taken as a mapping function from this boundary to another arbitrary one. The resulting integral equation for the mapping function is, however, not as easy to solve numerically as when the boundary C is a circle.

Once the conformal correspondence between two boundaries is known, corresponding points outside the boundaries can be determined by the Cauchy integral formula (44). It is noted that the Cauchy integral gives the correspondence of individual pairs of points rather than the correspondence of entire boundaries at once, which is given by the Fourier series representation. Furthermore, the possibility exists of determining pairs of corresponding points inside the given boundaries by the Cauchy integral, that is, of analytically continuing the conformal transformation beyond the original domains. For if the transformation from a boundary C in a p-plane to a boundary C' in a p'-plane were known, the outside regions corresponding, then the correspondence between a boundary A internal to C and a boundary A' internal to C', if it existed, could be determined by an application of the Cauchy integral formula to the region bounded by A and C.

For example, if the boundaries A and C are taken as concentric circles and the mapping function as

$$
\begin{aligned}
f(p) &= \log \frac{p'}{p} \\
&= \psi - i\epsilon = (\psi - \chi) - i(\varphi - \theta) \qquad (51)
\end{aligned}
$$

in the notation of figure 15, the Cauchy integral formula applied to the annular region in the p-plane (assumed free of singularities of the mapping function) yields, in the limit as the variable point p approaches the inner circle A,

$$
\begin{aligned}
\psi_1(\varphi_1') = \frac{1}{2\pi}\int_0^{2\pi} \epsilon_1(\varphi_1) \cot \frac{\varphi_1 - \varphi_1'}{2} d\varphi_1 \\
- \frac{1}{2\pi}\int_0^{2\pi} \frac{\epsilon_o(\varphi_o) \sin\left(\varphi_o - \varphi_1'\right) - \psi_o(\varphi_o) \sinh\left(\chi_o - \chi_1\right)}{\cosh\left(\chi_o - \chi_1\right) - \cos\left(\varphi_o - \varphi_1'\right)} d\varphi_o \qquad (52a)
\end{aligned}
$$

$$
\begin{aligned}
\epsilon_1(\varphi_1') = - \frac{1}{2\pi}\int_0^{2\pi} \psi_1(\varphi_1) \cot \frac{\varphi_1 - \varphi_1'}{2} d\varphi_1 \\
+ \frac{1}{2\pi}\int_0^{2\pi} \frac{\psi_o(\varphi_o) \sin\left(\varphi_o - \varphi_1'\right) + \epsilon_o(\varphi_o) \sinh\left(\chi_o - \chi_1\right)}{\cosh\left(\chi_o - \chi_1\right) - \cos\left(\varphi_o - \varphi_1'\right)} d\varphi_o \qquad (52b)
\end{aligned}
$$

In addition, the condition of regularity of the function f(p) in the annular region yields the auxiliary conditions

$$\left.\begin{aligned}\frac{1}{2\pi}\int_0^{2\pi}\epsilon_1 d\varphi_1 &= \frac{1}{2\pi}\int_0^{2\pi}\epsilon_o d\varphi_o\\ \frac{1}{2\pi}\int_0^{2\pi}\Psi_1 d\varphi_1 &= \frac{1}{2\pi}\int_0^{2\pi}\Psi_o d\varphi_o\end{aligned}\right\}\qquad(53)$$

In the problem under consideration, the mapping function

$$\psi_o(\varphi_o) - i\epsilon_o(\varphi_o)$$

for the outer boundaries is known. The radii e^{χ_o}, e^{χ_1} of the concentric circles are given. The second integrals of equations (52) are thus known functions of φ_1'. Equations (52a) and (52b) therefore constitute a pair of integral equations, similar to those of Theodorsen-Garrick, for the mapping function $\Psi_1(\varphi_1) - i\epsilon_1(\varphi_1)$, pertaining to the inner boundaries.

It is noted that if the variable point p of the Cauchy integral formula for the annular region is made to approach the outer boundary C, then two additional integral equations similar to equations (52a) and (52b) are obtained. These equations, together with equations (53), are a generalization to the case of ring regions of the corresponding Theodorsen-Garrick equations for simply connected regions and can be used for the conformal mapping of near circular ring regions.

REFERENCES

1. Mutterperl, William: A Solution of the Direct and Inverse Potential Problems for Arbitrary Cascades of Airfoils. NACA ARR No. L4K22b, 1944.

2. Theodorsen, T., and Garrick, I. E.: General Potential Theory of Arbitrary Wing Sections. NACA Rep. No. 452, 1933.

3. Millikan, Clark B.: An Extended Theory of Thin Airfoils and Its Application to the Biplane Problem. NACA Rep. No. 362, 1930.

4. Allen, H. Julian: General Theory of Airfoil Sections Having Arbitrary Shape or Pressure Distribution. NACA ACR No. 3G29, 1943.

5. Garrick, I. E.: Determination of the Theoretical Pressure Distribution for Twenty Airfoils. NACA Rep. No. 465, 1933.

6. Gebelein, H.: Theory of Two-Dimensional Potential Flow about Arbitrary Wing Sections. NACA TM No. 886, 1939.

7. Betz, A.: Modification of Wing-Section Shape to Assure a Predetermined Change in Pressure Distribution. NACA TM No. 767, 1935.

8. Hussmann, Albrecht: Rechnerische Verfahren zur harmonischen Analyse und Synthese. Julius Springer (Berlin), 1938.

9. Garrick, I. E.: Potential Flow about Arbitrary Biplane Wing Sections. NACA Rep. No. 542, 1936.

10. von Kármán, Th., and Burgers, J. M.: General Aerodynamic Theory - Perfect Fluids. Application of the Theory of Conformal Transformation to the Investigation of the Flow around Airfoil Profiles. Vol. II of Aerodynamic Theory, div. E, ch. II, pt. B. W. F. Durand, ed., Julius Springer (Berlin), 1935, p. 91.

11. Hurwitz, Adolf, and Courant, R.: Allgemeine Funktionentheorie und elliptische Funktionen, and Geometrische Funktionentheorie. Bd. III of Mathematischen Wissenschaften. Julius Springer (Berlin), 1929, p. 335.

12. Bergman, Stefan: Partial Differential Equations, Advanced Topics. Advanced Instruction and Research in Mechanics, Brown Univ., Summer 1941.

TABLE I

CARTESIAN MAPPING FUNCTION FOR SYMMETRICAL

30-PERCENT THICKNESS JOUKOWSKI PROFILE

φ (radians)	Δx_o	Δy_o	$d\Delta x_o/d\varphi$	$d\Delta y_o/d\varphi$
$0 \times \frac{\pi}{12}$	-0.319	0	0	0.375
1	-.304	.0964	.119	.355
2	-.258	.182	.226	.296
3	-.190	.250	.309	.206
4	-.101	.287	.352	.0894
5	-.00724	.295	.352	-.0351
6	.0798	.270	.304	-.149
7	.148	.218	.212	-.238
8	.189	.150	.0916	-.272
9	.197	.0810	-.0261	-.240
10	.179	.0291	-.0958	-.149
11	.154	.00412	-.0824	-.0346
12	.142	0	0	0

TABLE II

CONSTANTS USED WITH CMF OF TABLE I

Profile	T	λu_t	τ	r	φ_N (deg)	φ_T (deg)	u_t
Joukowski	0.30	1.000	0.0887	1.230	0	180	1.000
Derived	.24	.805	.0716	1.185	0	180	.835
Derived	.12	.402	.0357	1.0928	0	180	.453

NATIONAL ADVISORY COMMITTEE FOR AERONAUTICS

TABLE III

CMF FOR 6-PERCENT-CAMBER CIRCULAR-ARC PROFILE

φ (radians)	Δx_o	Δy_o	$d\Delta x_o/d\varphi$	$d\Delta y_o/d\varphi$
$6 \times \frac{\pi}{12}$	0	0.120	0.108	0
7	.0270	.114	.0960	-.0484
8	.0482	.0953	.0638	-.0871
9	.0592	.0694	.0171	-.109
10	.0565	.0405	-.0363	-.106
11	.0408	.0160	-.0844	-.0781
12	.0142	.00169	-.115	-.0279
13	-.0170	.00246	-.117	.0346
14	-.0439	.0194	-.0852	.0926
15	-.0587	.0490	-.0239	.128
16	-.0552	.0828	.0506	.123
17	-.0335	.110	.113	.0756
18	0	.120	.136	0

TABLE IV

CONSTANTS USED WITH CMF OF TABLE III

Profile	C (percent)	u_c	λu_c	τ	r	φ_N (deg)	φ_T (deg)	α_I (deg)	$c_{l_{ideal}}$
Derived	3	0.502	0.501	0	1.0052	-3.37	183.37	0	0.37
Circular arc	6	1.000	1.000	0	1.0072	-6.84	186.84	0	.75
Derived	9	1.502	1.499	0	1.0050	-10.26	190.26	0	-------

NATIONAL ADVISORY COMMITTEE FOR AERONAUTICS

TABLE V

THE DIRECT CMF METHOD FOR THE NACA 6512 AIRFOIL[a]

NATIONAL ADVISORY COMMITTEE FOR AERONAUTICS

Initial Approximation

φ (radians)	Δx_o	Δy_o	$\frac{d\Delta x_o}{d\varphi}$	$\frac{d\Delta y_o}{d\varphi}$	x_1	k_o	v_o ($c_l = 1.5$)
$0 \times \frac{\pi}{12}$	-0.145	0.0018	-0.126	0.183	0.992	0.201	1.633
1	-.168	.0565	-.0438	.229	.931	.364	1.600
2	-.166	.118	.0520	.236	.823	.508	1.596
3	-.142	.177	.144	.203	.672	.605	1.651
4	-.0935	.221	.211	.131	.493	.685	1.656
5	-.0325	.244	.248	.0388	.288	.742	1.625
6	.0324	.241	.241	-.0606	.0678	.783	1.546
7	.0898	.213	.191	-.150	-.160	.804	1.428
8	.129	.165	.107	-.206	-.386	.791	1.291
9	.145	.109	.0081	-.216	-.599	.727	1.156
10	.134	.0561	-.0786	-.122	-.784	.582	1.059
11	.107	.0192	-.126	-.0895	-.921	.382	.958
12	.0730	.0018	-.126	-.0302	-.993	.118	.891
13	.0439	.0010	-.0948	.0239	-.984	.174	.853
14	.0246	.0094	-.0543	.0410	-.894	.452	.834
15	.0156	.0207	-.0155	.0432	-.728	.694	.814
16	.0162	.0297	.0182	.0245	-.499	.883	.793
17	.0236	.0319	.0368	-.0138	-.226	.999	.773
18	.0324	.0218	.0252	-.0606	.0678	1.024	.759
19	.0337	.0008	-.0199	-.0970	.354	.952	.750
20	.0195	-.0263	-.0872	-.0987	.555	.792	.742
21	-.0128	-.0479	-.151	-.0566	.801	.572	.711
22	-.0566	-.0528	-.185	.0186	.933	.332	.551
23	-.105	-.0364	-.177	.106	.994	.138	.493

[a]CMF's of table V are with reference to chord rotated 0.88° counterclockwise from "longest-line" chord.

TABLE V

THE DIRECT CMF METHOD FOR THE NACA 6512 AIRFOIL[a] - Continued

NATIONAL ADVISORY COMMITTEE FOR AERONAUTICS

First approximation

φ (radians)	Δy_1	δy_1	dx_1	$\frac{d\delta x_1}{d\varphi}$	$\frac{d\delta y_1}{d\varphi}$	Δx_1	$\frac{d\Delta x_1}{d\varphi}$	$\frac{d\Delta y_1}{d\varphi}$	x_2	k_1	v_1 (c_l = 1.5)
$0 \times \frac{\pi}{12}$	0.0018	0	-0.0057	0.0446	0.0151	-0.151	-0.0812	0.198	0.995	0.192	1.680
1	.055	-.0016	.0069	.0429	-.0281	-.161	-.0009	.201	.947	.316	1.821
2	.106	-.0123	.0138	.0092	-.0490	-.153	.0612	.187	.844	.476	1.692
3	.153	-.0243	.0113	-.0210	-.0383	-.130	.123	.164	.689	.615	1.617
4	.189	-.0319	.0024	-.0428	-.0203	-.091	.169	.111	.498	.722	1.565
5	.209	-.0347	-.0103	-.0542	0	-.043	.194	.0388	.278	.793	1.517
6	.213	-.0276	-.0248	-.0398	.0486	.0076	.201	-.0120	.0406	.819	1.475
7	.200	-.0126	-.0312	-.0088	.0593	.0586	.182	-.0902	-.196	.806	1.422
8	.170	.0030	-.0292	.0268	.0573	.100	.134	-.150	-.423	.758	1.348
9	.125	.0163	-.0179	.0550	.0321	.127	.063	-.184	-.627	.672	1.253
10	.075	.0189	-.0068	.0668	-.0115	.134	-.0118	-.133	-.797	.524	1.180
11	.030	.0108	.0113	.0270	-.0410	.118	-.0988	-.131	-.924	.367	1.002
12	.003	.0012	.0134	-.0062	-.0258	.0864	-.132	-.0560	-.993	.129	.828
13	0	-.002	.0120	.0014	-.0039	.0559	-.0934	.0200	-.986	.176	.835
14	.0057	-.0037	.0137	.0076	-.0061	.0383	-.0467	.0349	-.892	.459	.819
15	.015	-.0057	.0156	.0099	-.0088	.0312	-.0056	.0344	-.722	.703	.804
16	.020	-.0097	.0199	.0145	-.0245	.0361	.0327	0	-.487	.895	.782
17	.014	-.0179	.0218	0	-.0367	.0454	.0368	-.0505	-.210	1.0	.774
18	-.007	-.0288	.0192	-.0214	-.0429	.0516	.0038	-.104	.0846	1.008	.774
19	-.035	-.0358	.0067	-.0436	-.0065	.0404	-.0635	-.104	.361	.914	.786
20	-.059	-.0327	-.0030	-.0344	.0153	.0165	-.122	-.0834	.606	.760	.779
21	-.078	-.0301	-.0117	-.0317	.0191	-.0245	-.183	-.0375	.795	.544	.758
22	-.071	-.0182	-.0189	-.0019	-.0496	-.0755	-.187	.0682	.921	.337	.561
23	-.043	-.0066	-.0146	.0262	.0322	-.119	-.151	.138	.989	.175	.350

[a]CMF's of table V are with reference to chord rotated 0.88° counterclockwise from "longest-line" chord.

TABLE V

THE DIRECT CMF METHOD FOR THE NACA 6512 AIRFOIL[a] - Concluded

NATIONAL ADVISORY COMMITTEE FOR AERONAUTICS

Second approximation

φ (radians)	Δy_2	δy_2	δx_2	$\frac{d\delta x_2}{d\varphi}$	$\frac{d\delta y_2}{d\varphi}$	Δx_2	$\frac{d\Delta x_2}{d\varphi}$	$\frac{d\Delta y_2}{d\varphi}$	x_3	k_2	v_2 ($c_l = 1.5$)
$0 \times \frac{\pi}{12}$	-0.0057	-0.0075	0.0043	-0.0064	-0.0138	-0.146	-0.0876	0.184	0.996	0.183	1.780
1	.045	-.010	.0005	-.0198	.0018	-.160	-.0207	.203	.943	.332	1.744
2	.098	-.008	-.0041	-.0095	.0138	-.157	.0517	.201	.836	.488	1.656
3	.149	-.004	-.0050	0	.0111	-.135	.123	.175	.681	.617	1.615
4	.188	-.001	-.0039	.0092	.0103	-.0950	.178	.121	.492	.714	1.584
5	.210	.001	-.0004	.0187	0	-.0432	.212	.0388	.276	.775	1.552
6	.212	-.0015	.0031	.0069	-.0130	.0107	.208	-.0250	.0426	.813	1.487
7	.195	-.005	.0032	-.0057	-.0130	.0618	.177	-.1032	-.193	.812	1.411
8	.162	-.008	.0006	-.0160	-.0057	.1006	.118	-.1559	-.423	.773	1.320
9	.118	-.0075	-.0037	-.0141	.0069	.1229	.0490	-.1769	-.629	.682	1.231
10	.071	-.004	-.0062	0	.0160	.1273	-.0118	-.1174	-.802	.522	1.180
11	.030	0	-.0046	.0133	.0047	.1136	-.0855	-.1258	-.926	.354	1.030
12	.003	0	-.0020	-.0036	-.0033	.0844	-.136	-.0593	-.994	.134	.778
13	0	0	-.0015	.0031	-.0014	.0544	-.0903	.0186	-.985	.178	.840
14	.006	0	-.0006	.0031	0	.0378	-.0437	.0349	-.891	.462	.819
15	.015	0	-.0002	.0019	0	.0310	-.0037	.0344	-.721	.705	.804
16	.020	0	.0009	.0025	-.0027	.0370	.0352	-.0027	-.486	.898	.781
17	.013	-.001	.0008	-.0008	0	.0462	.0360	-.0505	-.209	.999	.774
18	-.009	.001	.0010	.0067	.0076	.0526	.0105	-.0959	.0845	1.014	.768
19	-.036	-.001	.0054	0	-.0191	.0458	-.0635	-.123	.365	.915	.782
20	-.064	-.005	.0015	-.0076	0	.0180	-.129	-.0834	.605	.753	.783
21	-.078	0	.0008	.0015	0	-.0237	-.182	-.0375	.792	.545	.751
22	-.073	-.002	.0055	.0088	-.0107	-.0700	-.178	.0575	.923	.343	.540
23	-.048	-.005	.0047	-.0024	-.0022	-.115	-.153	.136	.989	.172	.379

[a]CMF's of table V are with reference to chord rotated 0.88° counterclockwise from "longest-line" chord.

TABLE VI

CONSTANTS USED WITH CMF's OF TABLE V

[All angles are given with reference to "longest-line" chord of airfoil. "Longest-line" chord is rotated clockwise 53' with respect to "x-axis" chord.]

Approximation	r	τ	β_T	β_N	α ($c_l = 1.5$)
Initial	1.1013	0.0354	6° 58'	7° 25'	5° 33'
1st	1.1128	.0330	7° 4'	4° 50'	5° 19'
2nd	1.1102	.0319	6° 55'	5° 4'	5° 30'
Theodorsen-Garrick, 1st approximation	1.119	------	7° 4'	7° 39'	5° 21'

NATIONAL ADVISORY
COMMITTEE FOR AERONAUTICS

TABLE VII.- INVERSE CMF METHOD FOR SYMMETRICAL PROFILE VELOCITY DISTRIBUTION

	Initial CMF				First increment CMF				First approximation						
φ (radians)	Δx_o	Δy_o	$\frac{d\Delta x_o}{d\varphi}$	$\frac{d\Delta y_o}{d\varphi}$	δx_1	δy_1	$\frac{d\delta x_1}{d\varphi}$	$\frac{d\delta y_1}{d\varphi}$	Δx_1	Δy_1	$\frac{d\Delta x_1}{d\varphi}$	$\frac{d\Delta y_1}{d\varphi}$	x_1	k	v
$0 \times \frac{\pi}{12}$	-0.129	0	0	0.151	0	0	0	-0.0134	-0.1192	0	0	0.137	1.000	0.126	0
1	-.122	.0388	.0480	.143	.0006	-.0059	-.0054	-.0339	-.1123	.0329	.0426	.109	.969	.241	1.073
2	-.104	.0734	.0909	.119	-.0059	-.0136	-.0384	-.0165	-.1003	.0598	.0525	.102	.872	.462	1.083
3	-.0763	.101	.124	.0830	-.0163	-.0139	-.0389	.0119	-.0883	.0867	.0853	.0949	.715	.635	1.113
4	-.0405	.116	.141	.0359	-.0249	-.0074	-.0239	.0370	-.0561	.1083	.1174	.0729	.516	.761	1.137
5	-.0029	.119	.142	-.0141	-.0275	.0039	.0043	.0466	-.0211	.1224	.1459	.0325	.288	.833	1.160
6	.0321	.109	.122	-.0601	-.0214	.0151	.0437	.0309	.0200	.1236	.1661	-.0292	.0463	.849	1.178
7	.0597	.0877	.0854	-.0957	-.0093	.0164	.0362	-.0179	.0597	.1041	.1216	-.114	-.197	.861	1.122
8	.0759	.0602	.0368	-.110	-.0042	.0114	.0099	-.0137	.0810	.0716	.0467	-.123	-.439	.831	1.042
9	.0791	.0326	-.0105	-.0963	-.0015	.0079	.0071	-.0156	.0869	.0405	-.0034	-.112	-.659	.718	.984
10	.0720	.0117	-.0385	-.0597	-.0011	.0046	.0006	-.0076	.0802	.0163	-.0379	-.0673	-.840	.538	.928
11	.0619	.0017	-.0331	-.0139	-.0005	.0028	.0044	-.0091	.0707	.0045	-.0287	-.0230	-.958	.286	.906
12	.0572	0	0	0	0	0	0	-.0110	.0665	0	0	-.0110	-1.000	-----	.895

$r_o = 1.0928$

$\tau_o = 0.0357$

$\varphi_{N_o} = 0$

$\varphi_{T_o} = 180^\circ$

$r_1 = 1.0929$

$\tau_1 = 0.0263$

$\varphi_{N_1} = 0$

$\varphi_{T_o} = 180^\circ$

NATIONAL ADVISORY
COMMITTEE FOR AERONAUTICS

TABLE VIII.- INVERSE CMF METHOD FOR a = 1 CAMBER LINE VELOCITY DISTRIBUTION

NATIONAL ADVISORY
COMMITTEE FOR AERONAUTICS

φ (radians)	δx_1	δy_1	$\frac{d\delta x_1}{d\varphi}$	$\frac{d\delta y_1}{d\varphi}$	Δx_1	Δy_1	$\frac{d\Delta x_1}{d\varphi}$	$\frac{d\Delta y_1}{d\varphi}$	x_1	k	v (c_l = 0.67)	v (Modified distribution for c_l = 0.8)
$6 \times \frac{\pi}{12}$	0	-0.0234	-0.0517	0	0	0.0823	0.0556	0	0	0.940	1.171	1.194
7	-.0122	-.0192	-.0375	.0286	.0148	.0805	.0583	-.0197	-.245	.913	1.181	1.203
8	-.0194	-.0101	-.0180	.0401	.0287	.0710	.0457	-.0469	-.474	.820	1.183	1.208
9	-.0210	.0012	.0069	.0435	.0381	.0564	.0239	-.0649	-.672	.689	1.185	1.214
10	-.0161	.0111	.0286	.0289	.0403	.0375	-.0077	-.0769	-.829	.514	1.183	1.222
11	-.0075	.0154	.0332	.0031	.0331	.0173	-.0511	-.0748	-.937	.321	1.147	1.210
12	-.0013	.0141	.0123	-.0056	.0127	.0018	-.1025	-.0334	-.992	.103	.988	1.177
13	.0018	.0154	.0206	.0134	-.0152	.0037	-.0963	.0479	-.985	.171	.899	.780
14	.0114	.0166	.0470	-.0130	-.0325	.0219	-.0381	.0794	-.902	.473	.840	.798
15	.0217	.0076	.0256	-.0506	-.0369	.0424	-.0017	.0774	-.747	.711	.843	.815
16	.0234	-.0072	-.0131	-.0580	-.0317	.0614	.0374	.0654	-.534	.907	.838	.816
17	.0151	-.0204	-.0487	-.0382	-.0183	.0753	.0636	.0374	-.278	1.033	.835	.815
18	0	-.0256	-.0618	0	0	.0802	.0740	0	0	1.069	.832	.813

$r_1 = 1.0043$ $\qquad$ $\varphi_{T_1} = 186.10^\circ$

$\tau_1 = 0$ $\qquad$ $c_l = 0.67$

$\varphi_{N_1} = -6.10^\circ$

TABLE IX

THE USE OF THE RUNGE SCHEDULE IN THE ANALYSIS

AND SYNTHESIS OF CONJUGATE FOURIER SERIES

Process	Entry in schedule		Result
Direct method			
Analysis	Enter $\frac{\delta y}{12}$ for y_n		a_n, b_n
Synthesis	Enter in d_n spaces	Enter in D_n spaces	
	$-b_n$	a_n	δx
	na_n	nb_n	$d\delta x/d\varphi$
	nb_n	$-na_n$	$d\delta y/d\varphi$
Inverse method of potentials			
Analysis	Enter $\frac{\delta x}{12}$ for y_n		a_n, b_n
Synthesis	Enter in d_n spaces	Enter in D_n spaces	
	b_n	$-a_n$	δy
	nb_n	$-na_n$	$d\delta x/d\varphi$
	$-na_n$	$-nb_n$	$d\delta y/d\varphi$
Inverse method of derivatives			
Analysis	Enter $\frac{1}{12}\frac{d\Delta x}{d\varphi}$ for y_n		a_n, b_n
Synthesis	Enter in d_n spaces	Enter in D_n spaces	
	b_n	$-a_n$	$d\Delta y/d\varphi$
	$-b_n/n$	a_n/n	Δx
	a_n/n	b_n/n	Δy

NATIONAL ADVISORY
COMMITTEE FOR AERONAUTICS.

TABLE X

THE USE OF THE RUNGE SCHEDULE IN THE DIRECT METHOD FOR THE NACA 6512 AIRFOIL; FIRST APPROXIMATION

(a) Analysis of $\delta y_1 \times 100$

Sum table for 24 ordinates

1 Analysis: Enter $\frac{y_n}{12}$ — Times 2 for synthesis

1	A	U + V	y_0 0	y_1 -0.0133	y_2 -0.103	y_3 -0.203	y_4 -0.266	y_5 -0.289	y_6 -0.230	y_7 -0.105	y_8 0.0250	y_9 0.136	y_{10} 0.158	y_{11} 0.0900	
2	B	U - V		y_{23} -0.0550	y_{22} -0.152	y_{21} -0.251	y_{20} -0.273	y_{19} -0.298	y_{18} -0.240	y_{17} -0.149	y_{16} -0.0808	y_{15} -0.0475	y_{14} -0.0308	y_{13} -0.0167	y_{12} 0.0100
3	A + B	U	d_0	d_1	d_2	d_3	d_4	d_5	d_6	d_7	d_8	d_9	d_{10}	d_{11}	d_{12}
4	A - B	V		D_1	D_2	D_3	D_4	D_5	D_6	D_7	D_8	D_9	D_{10}	D_{11}	

Times 2 for synthesis

Synthesis

Enter D in table 2b

Enter d in table 2a

2a: Beginning of synthesis calculation. Enter a_n

A	d_0 0	d_1 -0.0683	d_2 -0.254	d_3 -0.453	d_4 -0.538	d_5 -0.588	
B	d_{12} 0.0100	d_{11} 0.0733	d_{10} 0.127	d_9 0.0883	d_8 -0.0558	d_7 -0.254	d_6 -0.470
A + B	e_0	e_1	e_2	e_3	e_4	e_5	e_6
A - B	f_0	f_1	f_2	f_3	f_4	f_5	

Enter e in table 3a

Enter f in table 4a

2b Beginning of synthesis calculation. Enter b_n

A	D_1 0.0417	D_2 0.0492	D_3 0.0483	D_4 0.0067	D_5 0.0091	
B	D_{11} 0.107	D_{10} 0.188	D_9 0.183	D_8 0.106	D_7 0.0442	D_6 0.0100
A + B	F_1	F_2	F_3	F_4	F_5	F_6
A - B	E_1	E_2	E_3	E_4	E_5	

Enter F in table 4b

Enter E in table 3b

3a

A	e_0 0.0100	e_1 0.0050	e_2 -0.128	
B	e_6 -0.470	e_5 -0.842	e_4 -0.594	e_3 -0.365
A + B	g_0	g_1	g_2	g_3
A - B	h_0	h_1	h_2	

Enter g in table 5a

Enter h in table 6a

4a — f

A	+	f_0 -0.0100	f_1 -0.142	f_2 -0.381
B	−	f_4 -0.483	f_3 -0.542	
C	−		f_5 0.333	
A - B - C		l_0 0.473	l_1 0.733	

l

3b

A	E_1 -0.0650	E_2 -0.139	
B	E_5 -0.0351	E_4 -0.0991	E_3 -0.135
A + B	H_1	H_2	H_3
A - B	G_1 -0.0299	G_2 -0.0400	

Enter H in table 6b

G

4b — F

A	+		F_1 0.148	F_2 0.238
B	+	F_4 0.113	F_3 0.232	
C	−		F_5 0.0533	F_6 0.0100
A+B-C			L_1 0.327	L_2 0.228

L

5a — g

A	+	g_0 -0.460	g_1 -0.837
B	+	g_2 -0.722	g_3 -0.365
A + B		i_0 -1.182	i_1 -1.202

i

6a — h

A	+	h_0 0.480	h_1 0.847
B	−	h_2 0.467	
A - B		k_0 0.0134	

k

6b — H

A	+	H_1 -0.100	H_2 -0.238
B	−	H_3 -0.135	
A - B		K_1 0.0349	

K

NATIONAL ADVISORY
COMMITTEE FOR AERONAUTICS.

Product table for 24 ordinates

Product table for the cosine coefficients

$\mu\varrho\alpha$	$\frac{\cos\mu\varrho\alpha}{12}$	0		1		2		3		4		5		6	$\mu\varrho\alpha$	Check I	Check II	
0°	1.00000	$\frac{1}{2}i_0$	$\frac{1}{2}i_1$	f_0 0		h_0 0.0349		l_0		g_0 -0.0349	$-g_3$ 0.462	f_0 0		k_0	0°		II$_0$ -0.478	
15°	.96593				f_1 -0.439								f_5 -0.0607		15°		II$_1$ -0.749	
30°	.86603			f_2 0.357			h_1					$-f_2$ -0.357			30°		II$_2$ -0.391	
45°	.70711				f_3 -0.322				l_1				$-f_3$ 0.322		45°		II$_3$ 0.0327	
60°	.50000			f_4 0.0346		h_2 0.159				$-g_2$ -0.211	g_1 -0.247	f_4 0.0346			60°		II$_4$ 0.108	
75°	.25882				f_5 -0.0163								f_1 -0.117		75°		II$_5$ 0.0372	
Sum I		I$_0$ 0.194	II$_0$	I$_1$ 0.392	II$_1$	I$_2$ 0.194	II$_2$	I$_3$ -0.0692	II$_3$	I$_4$ -0.246	II$_4$	I$_5$ -0.323	II$_5$	I$_6$ -0.142		$\sum_0^5 I_n$ = ...	Σ = ...	Analysis
" II		II$_0$ -0.478		II$_1$ -0.775		II$_2$ -0.451		II$_3$ 0.0462		II$_4$ 0.215		II$_5$ 0.144		$-\frac{1}{2}k_0$		6 y_0 = ...	3d$_1$ = ...	
I + II		a_0 -0.284		a_1 -0.383		a_2 -0.257		a_3 -0.0230		a_4 -0.0309		a_5 -0.179		a_6 -0.284		$\sum_0^5 I_n$ = ... 0 ...	Σ = -5.144	Synthesis
I − II		a_{12} 0.672		a_{11} 1.167		a_{10} 0.645		a_9 -0.115		a_8 -0.461		a_7 -0.467		$-k_0$		6·d_0 = ±6b$_0$ ... 0 ...	3d$_1$ = -5.144	

Product table for the sine coefficients

$\mu\varrho\alpha$	$\frac{\sin\mu\varrho\alpha}{12}$	1		2		3		4		5		6	$\mu\varrho\alpha$	Check III	Check IV	
15°	.25882	F_1 -0.301								F_5 0.0407			15°	III$_1$ 0.134		
30°	.50000		F_2 0.713	H_1 -0.582							F_2 0.713		30°	III$_2$ 0.228	IV$_1$+IV$_5$ 0.727	
45°	.70711	F_3 0.668				L_1				$-F_3$ -0.668			45°	III$_3$ -0.187		
60°	.86603		F_4 -0.172		H_2			G_1	G_2		$-F_4$ 0.172		60°	III$_4$ -0.946	IV$_2$+IV$_4$ 2.200	
75°	.96593	F_5 0.152								F_1 -1.123			75°	III$_5$ -1.691		
90°	1.00000		F_6 0.0134	H_3 1.037			L_2				F_6 0.0134	K_1	90°	III$_6$ -1.100	IV$_3$ 1.413	
Sum III		III$_1$ 0.519	IV$_1$	III$_2$ 0.455	IV$_2$	III$_3$ -0.265	IV$_3$	III$_4$ -1.092	IV$_4$	III$_5$ -1.750	IV$_5$	III$_6$ -1.100		Σ = ...	Σ = ...	Analysis
" IV		IV$_1$ 0.55		IV$_2$ 1.178		IV$_3$ 1.413		IV$_4$ 1.363		IV$_5$ 0.899		$-\frac{1}{2}K_1$		3D$_1$ = ...	3D$_2$ = ...	
III + IV		b_1 1.074		b_2 1.633		b_3 1.148		b_4 0.270		b_5 -0.852		b_6 -2.200		Σ = -3.562	Σ = 4.340	Synthesis
III − IV		b_{11} -0.0358		b_{10} 0.722		b_9 -1.678		b_8 -2.455		b_7 -2.649		$-K_1$		3D$_1$ = -3.562	3D$_2$ = 4.340	

NATIONAL ADVISORY COMMITTEE FOR AERONAUTICS.

TABLE X

THE USE OF THE RUNGE SCHEDULE IN THE DIRECT METHOD FOR THE NACA 6512 AIRFOIL; FIRST APPROXIMATION - CONCLUDED

(b) Synthesis for $\delta x_1 \times 100$

Sum table for 24 ordinates

1 Analysis; Enter $\frac{y_n}{12}$; Times 2 for synthesis

	Analysis	Synthesis													
1	A	U + V	y_0 -0.569	y_1 0.691	y_2 1.376	y_3 1.125	y_4 0.240	y_5 -1.031	y_6 -2.484	y_7 -3.115	y_8 -2.916	y_9 -1.794	y_{10} -0.0769	y_{11} 1.131	
2	B	U - V		y_{23} -1.457	y_{22} -1.890	y_{21} -1.191	y_{20} -0.301	y_{19} 0.673	y_{18} 1.917	y_{17} 2.182	y_{16} 1.994	y_{15} 1.563	y_{14} 1.367	y_{13} 1.203	y_{12} 1.343
3	A + B	U	d_0 -0.284	d_1 -0.383	d_2 -0.257	d_3 -0.0230	d_4 -0.0309	d_5 -0.179	d_6 -0.284	d_7 -0.467	d_8 -0.461	d_9 -0.115	d_{10} 0.645	d_{11} 1.167	d_{12} 0.672
4	A - B	V		D_1 1.074	D_2 1.633	D_3 1.148	D_4 0.270	D_5 -0.952	D_6 -2.200	D_7 -2.649	D_8 -2.455	D_9 -1.678	D_{10} -0.722	D_{11} -0.0358	

Times 2 for synthesis

Enter D in table 2b

Enter d in table 2a

2a: Beginning of synthesis calculation. Enter a_n

A	d_0 0	d_1 -0.480	d_2 0.391	d_3 -0.459	d_4 0.0605	d_5 -0.0247	
B	d_{12}	d_{11} -0.0275	d_{10} -0.0212	d_9 -0.0035	d_8 -0.0097	d_7 0.0381	d_6 -0.0349
A + B	e_0	e_1	e_2	e_3	e_4	e_5	e_6
A - B	f_0	f_1	f_2	f_3	f_4	f_5	

Enter e in table 3a

Enter f in table 4a

2b: Beginning of synthesis calculation. Enter b_n

A	D_1 -1.187	D_2 1.447	D_3 0.991	D_4 -0.153	D_5 0.103	
B	D_{11} 0.249	D_{10} -0.0200	D_9 -0.0460	D_8 -0.0458	D_7 0.0542	D_6 0.0194
A + B	F_1	F_2	F_3	F_4	F_5	F_6
A - B	E_1	E_2	E_3	E_4	E_5	

Enter F in table 4b

Enter E in table 3b

3a

A	e_0 0	e_1 -0.507	e_2 0.370	
B	e_6 -0.0349	e_5 0.0134	e_4 0.0518	e_3 -0.462
A + B	g_0	g_1	g_2	g_3
A - B	h_0	h_1	h_2	

Enter g in table 5a

Enter h in table 6a

4a *f*

A	+	f_0 0	f_1 -0.452	f_2 0.413
B	-	f_4 0.0692	f_3 -0.455	
C	-		f_5 -0.0628	
A - B - C		l_0 -0.0692	l_1 0.0654	

l

3b

A	E_1 -1.212	E_2 1.467	
B	E_5 0.0489	E_4 -0.107	E_3 1.037
A + B	H_1	H_2	H_3
A - B	G_1 -1.261	G_2 1.573	

Enter H in table 6b

G

4b *F*

A	+		F_1 -1.162	F_2 1.427
B	+	F_4 -0.198	F_3 0.945	
C	-		F_5 0.157	F_6 0.0134
A+B-C			L_1 -0.395	L_2 1.413

L

5a *g*

A	+	g_0 -0.0349	g_1 -0.494
B	+	g_2 0.422	g_3 -0.462
A + B		i_0 0.387	i_1 -0.956

i

6a *h*

A	+	h_0 -0.0349	h_1 -0.521
B	-	h_2 0.318	
A - B		k_0 -0.284	

k

6b *H*

A	+	H_1 -1.163	H_2 1.360
B	-	H_3 1.037	
A - B		K_1 -2.200	

K

NATIONAL ADVISORY
COMMITTEE FOR AERONAUTICS.

Product table for 24 ordinates

Product table for the cosine coefficients

$\mu\varrho\alpha$	$\cos\frac{\mu\varrho\alpha}{12}$	0		1		2		3		4		5		6	$\mu\varrho\alpha$	Check I	Check II	
0°	1.00000	$\frac{1}{2}i_0$	$\frac{1}{2}i_1$	f_0 -0.0100		h_0 0.480		l_0		g_0 -0.460	$-g_3$ 0.365	f_0 -0.0100		k_0	0°		II_0 -0.601	
15°	.96593				f_1 -0.137								f_5 -0.322		15°		II_1 -0.586	
30°	.86603			f_2 -0.330			h_1					$-f_2$ 0.330			30°		II_2 0.635	
45°	.70711				f_3 -0.383				l_1				$-f_3$ 0.383		45°		II_3 0.367	
60°	.50000			f_4 -0.241		h_2 0.233				$-g_2$ 0.361	g_1 -0.418	f_4 -0.241			60°		II_4 -0.0267	
75°	.25882				f_5 -0.0863								f_1 -0.0367		75°		II_5 0.0064	
Sum I		I_0 -0.591	II_0	I_1 -0.581	II_1	I_2 0.713	II_2	I_3 0.473	II_3	I_4 0.0992	II_4	I_5 0.0786	II_5	I_6 0.0067		$\sum_0^6 I_n$ = -0.001	Σ = -0.205	Analysis
" II		II_0 -0.601		II_1 -0.606		II_2 0.733		II_3 0.519		II_4 0.0534		II_5 0.0245		$-\frac{1}{2}k_0$		$6y_0$ = 0	$3d_1$ = -0.205	
I + II		a_0 -1.192		a_1 -1.187		a_2 1.447		a_3 0.991		a_4 -0.153		a_5 0.103		a_6 0.0134		$\sum_0^6 I_n$ =	Σ =	Synthesis
I − II		a_{12} 0.0101		a_{11} 0.0249		a_{10} -0.0200		a_9 -0.0460		a_8 -0.0458		a_7 0.0542		$-k_0$		$6 \cdot d_0 = \pm 6b_0$	$3d_1$ =	

Product table for the sine coefficients

$\mu\varrho\alpha$	$\sin\frac{\mu\varrho\alpha}{12}$	1		2		3		4		5		6	$\mu\varrho\alpha$	Check III	Check IV	
15°	.25882	F_1 0.0384								F_5 0.0138			15°	III_1 0.0657		
30°	.50000		F_2 0.119	H_1 -0.0501							F_2 0.119		30°	III_2 -0.0926	IV_1+IV_5 0.129	
45°	.70711	F_3 0.164				L_1				$-F_3$ -0.164			45°	III_3 0.163		
60°	.86603		F_4 0.0974		H_2			G_1	G_2		$-F_4$ -0.0974		60°	III_4 -0.0224	IV_2+IV_4 -0.209	
75°	.96593	F_5 0.0515								F_1 0.143			75°	III_5 -0.0064		
90°	1.00000		F_6 0.0100	H_3 -0.135			L_2				F_6 0.0100	K_1	90°	III_6 0.0175	IV_3 0.228	
Sum III		III_1 0.254	IV_1	III_2 -0.185	IV_2	III_3 0.231	IV_3	III_4 -0.0259	IV_4	III_5 -0.0067	IV_5	III_6 0.0175		Σ = 0.125	Σ = 0.148	Analysis
" IV		IV_1 0.226		IV_2 -0.206		IV_3 0.228		IV_4 -0.0346		IV_5 0.0314		$-\frac{1}{2}K_1$		$3D_1$ = 0.125	$3D_2$ = 0.148	
III + IV		b_1 0.480		b_2 -0.391		b_3 0.459		b_4 -0.0605		b_5 0.0247		b_6 0.0349		Σ =	Σ =	Synthesis
III − IV		b_{11} 0.0275		b_{10} 0.0212		b_9 0.0035		b_8 0.0087		b_7 -0.0381		$-K_1$		$3D_1$ =	$3D_2$ =	

NATIONAL ADVISORY COMMITTEE FOR AERONAUTICS.

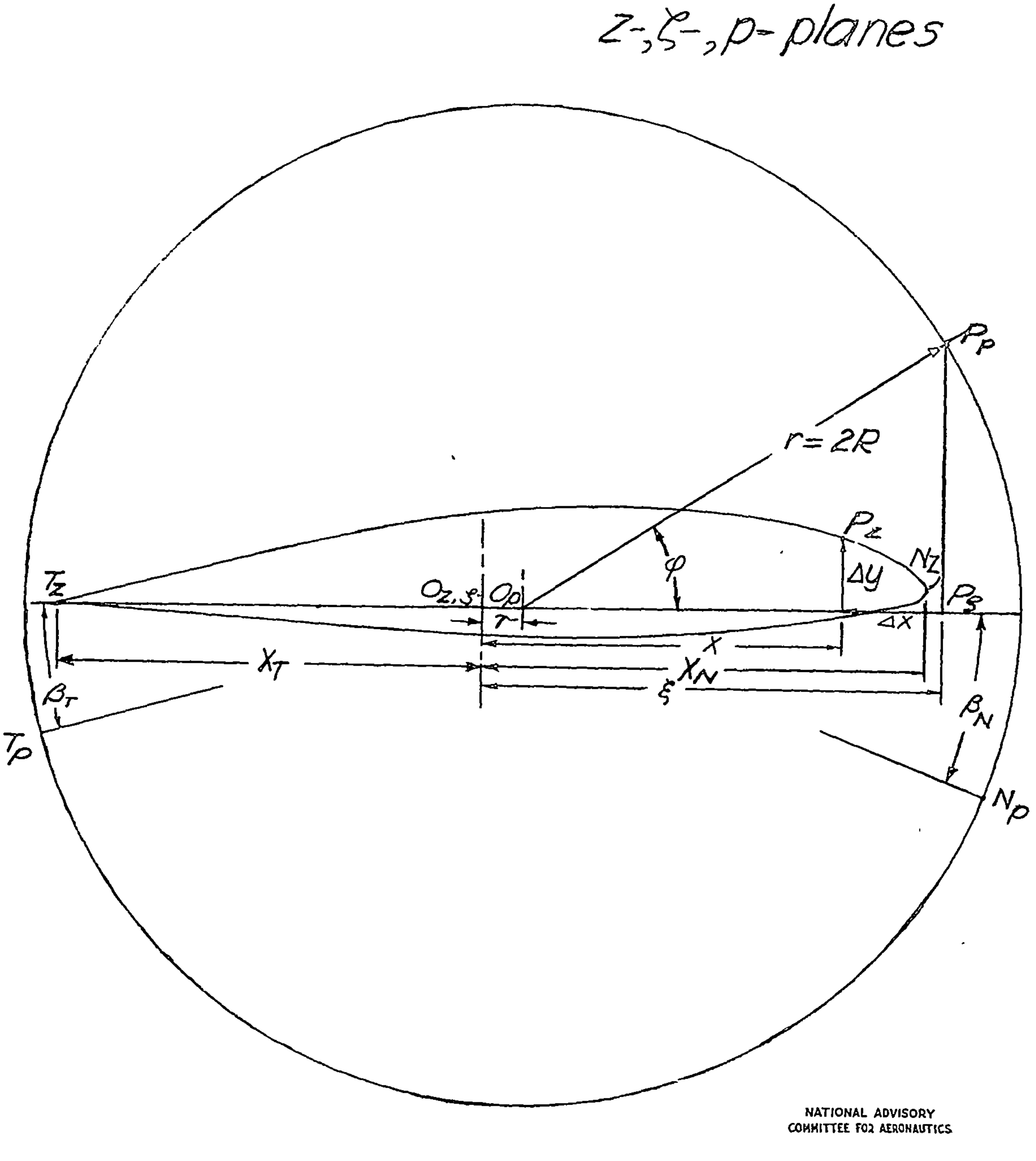

Figure 1.– Illustration of the Cartesian mapping function.

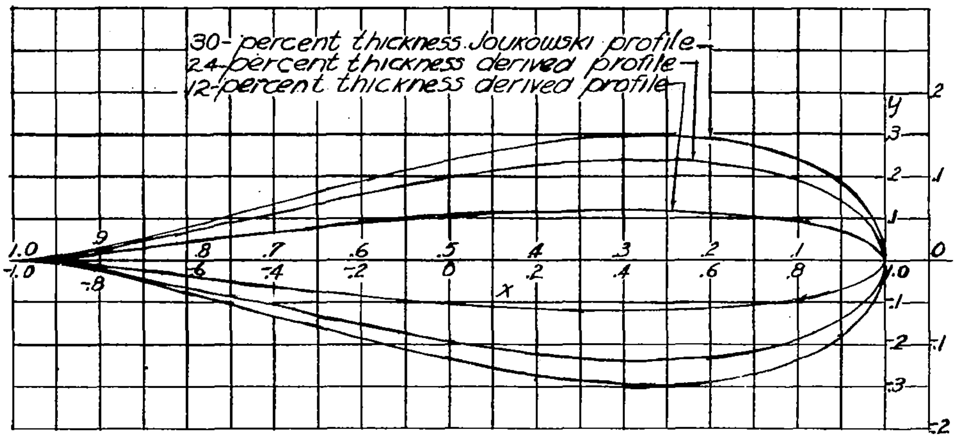

(a) Profiles.

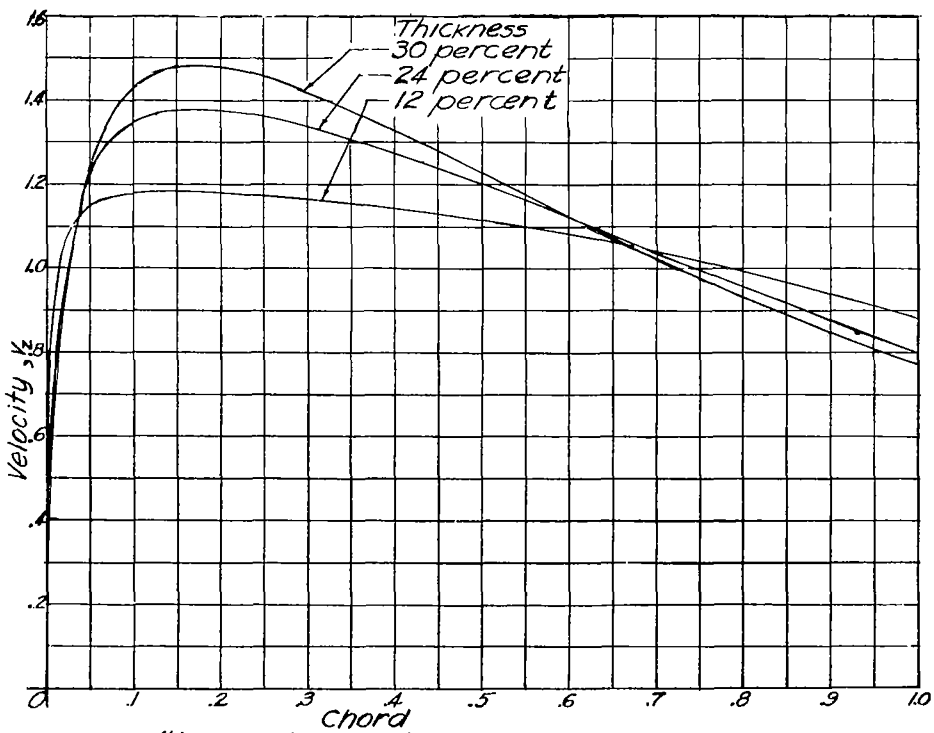

(b) Velocity distributions.

Figure 2.- Joukowski thickness form, derived thickness forms, and velocity distributions by method of Cartesian mapping function.

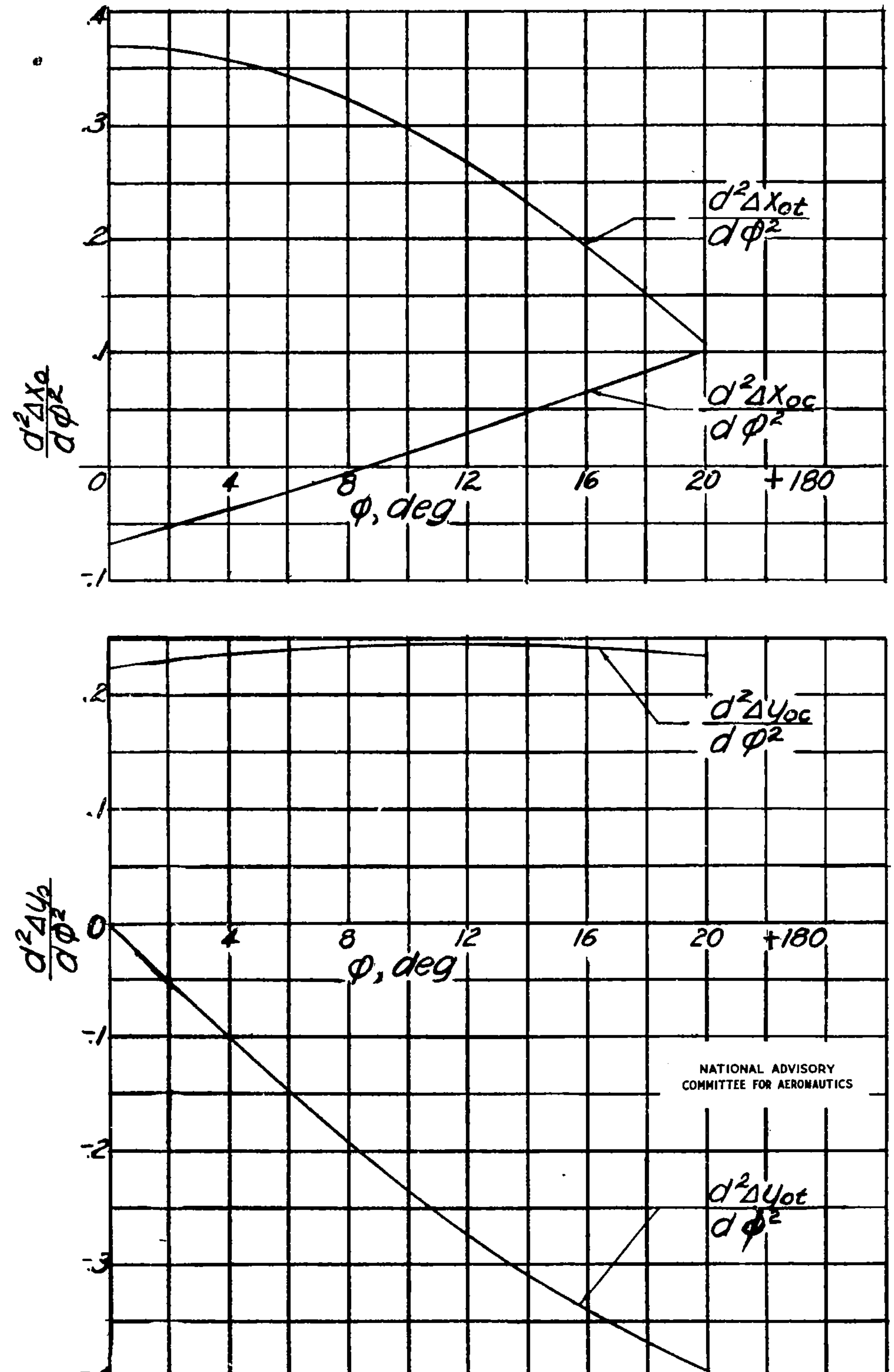

Figure 3.- Second derivatives of CMF's.

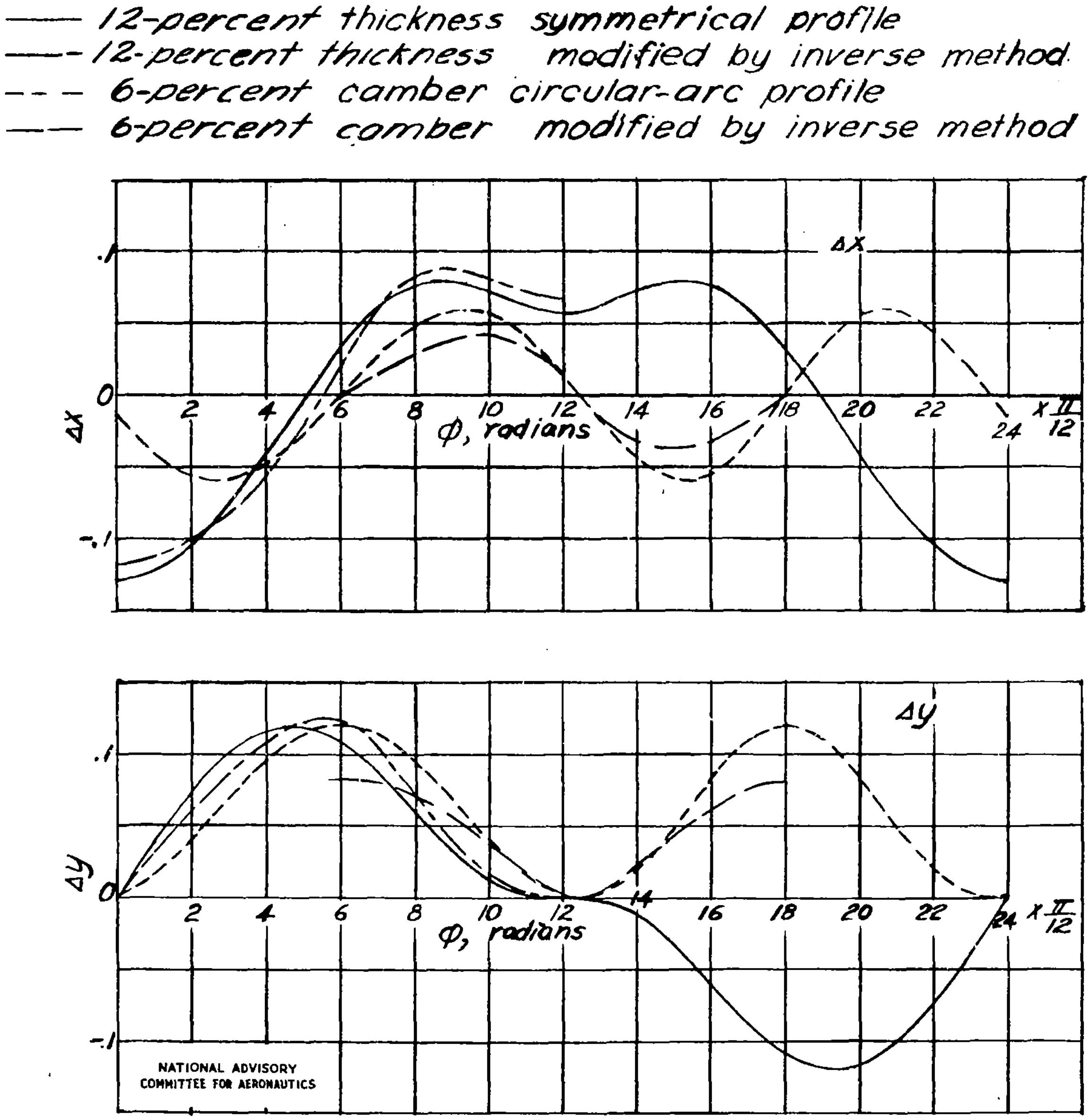

Figure 4.— Cartesian mapping functions.

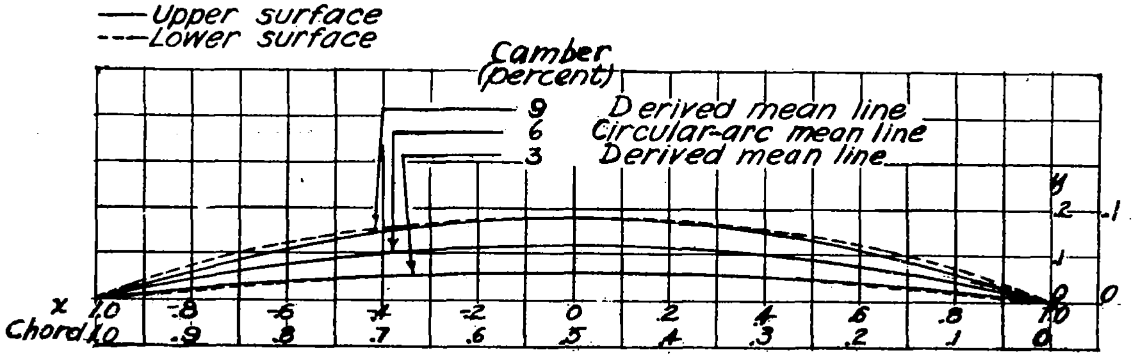

(a) Mean camber lines.

NATIONAL ADVISORY COMMITTEE FOR AERONAUTICS.

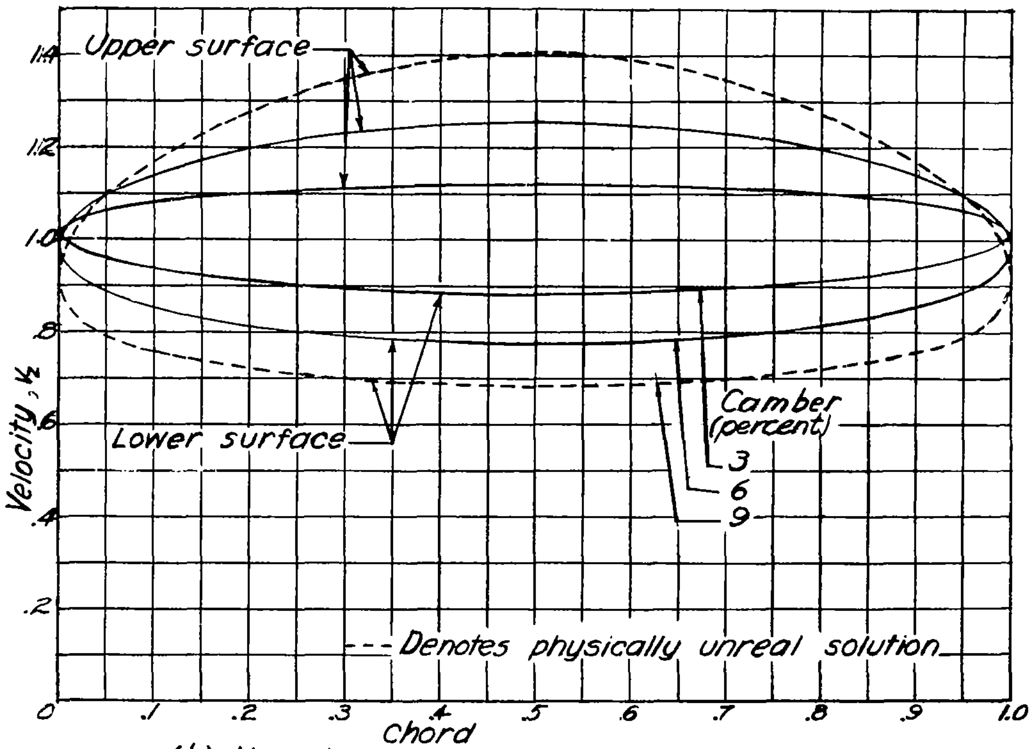

(b) Velocity distributions, $\alpha = 0$.

Figure 5.-Circular-arc mean line, derived mean lines, and velocity distributions by method of Cartesian mapping function.

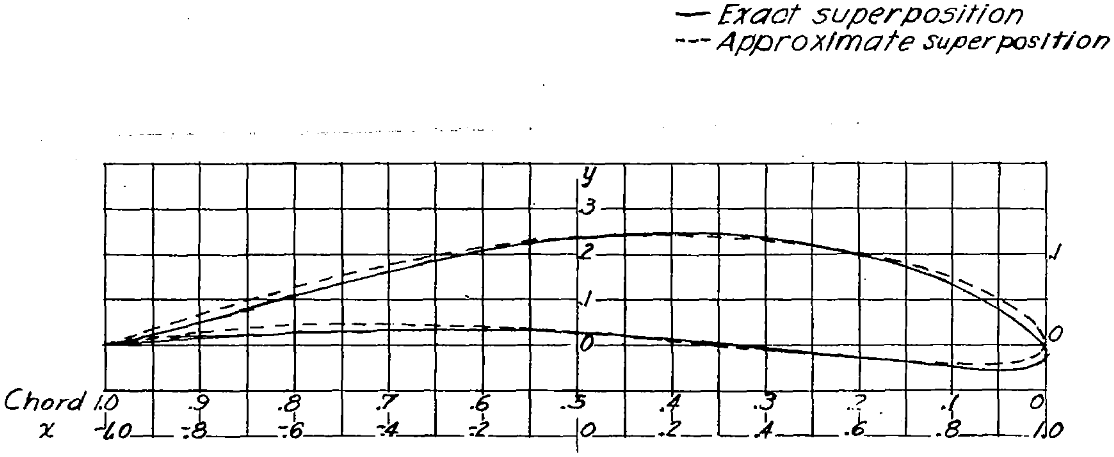

(a) Profiles.

NATIONAL ADVISORY COMMITTEE FOR AERONAUTICS

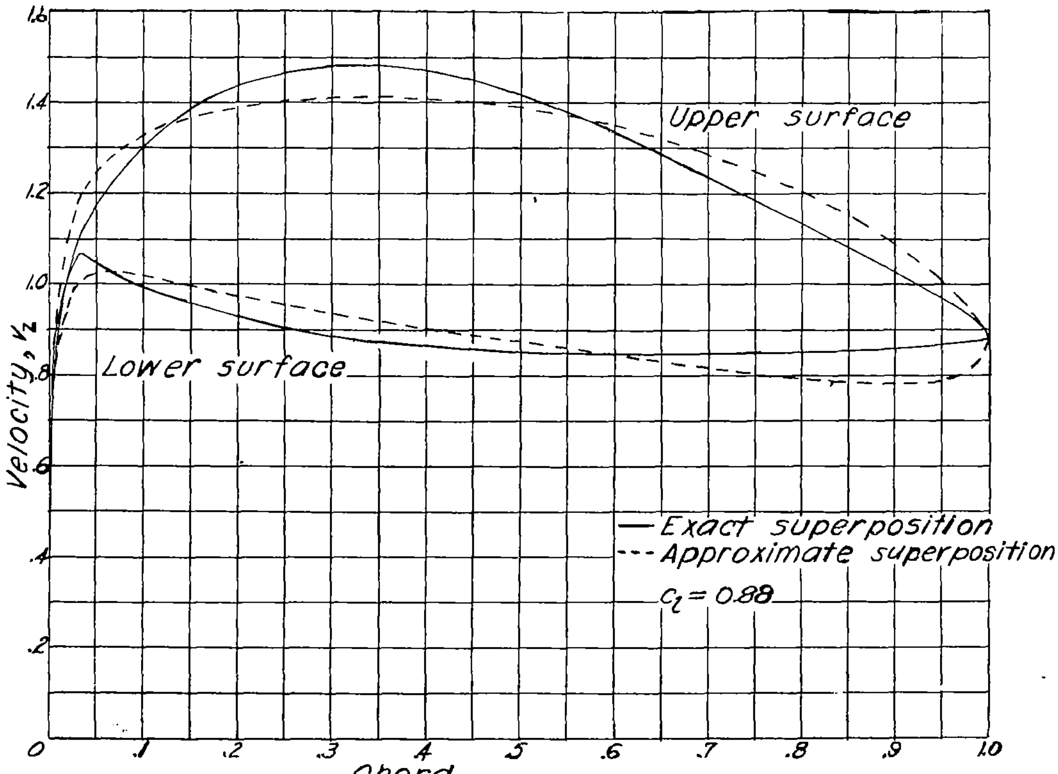

(b) Velocity distribution

Figure 6.- Superposition by CMF method and by thin-airfoil theory.

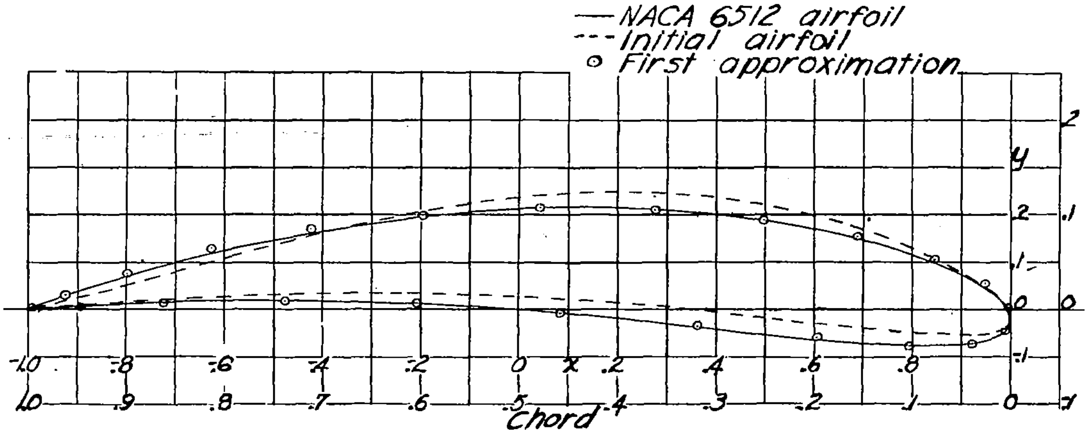

NATIONAL ADVISORY
COMMITTEE FOR AERONAUTICS

(a) Profiles.

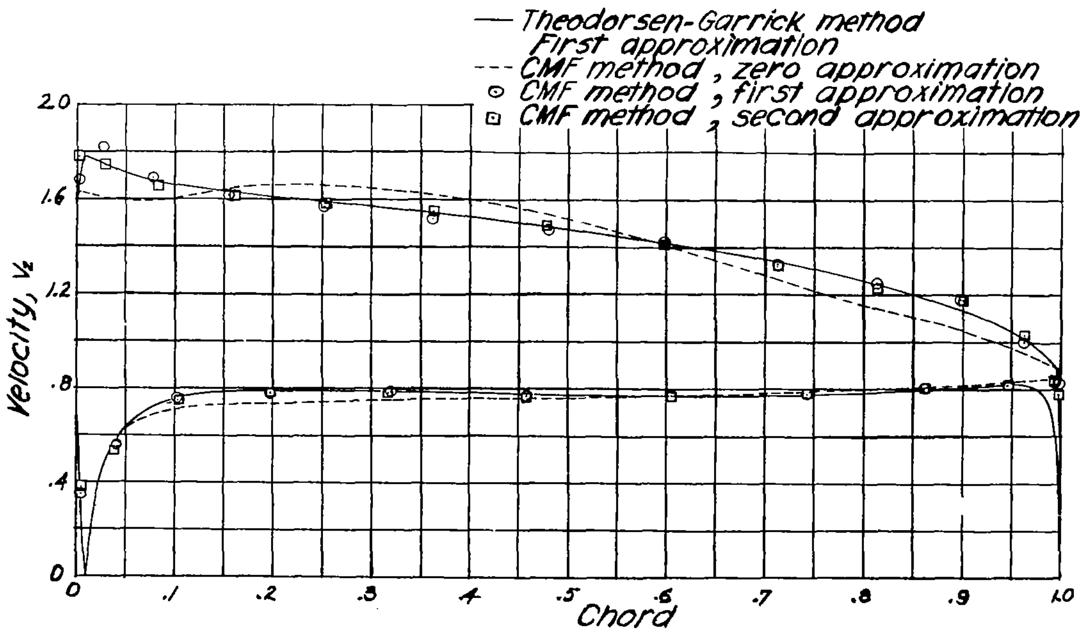

(b) Velocity distributions.

Figure 7.- Direct CMF method for NACA 6512 airfoil.

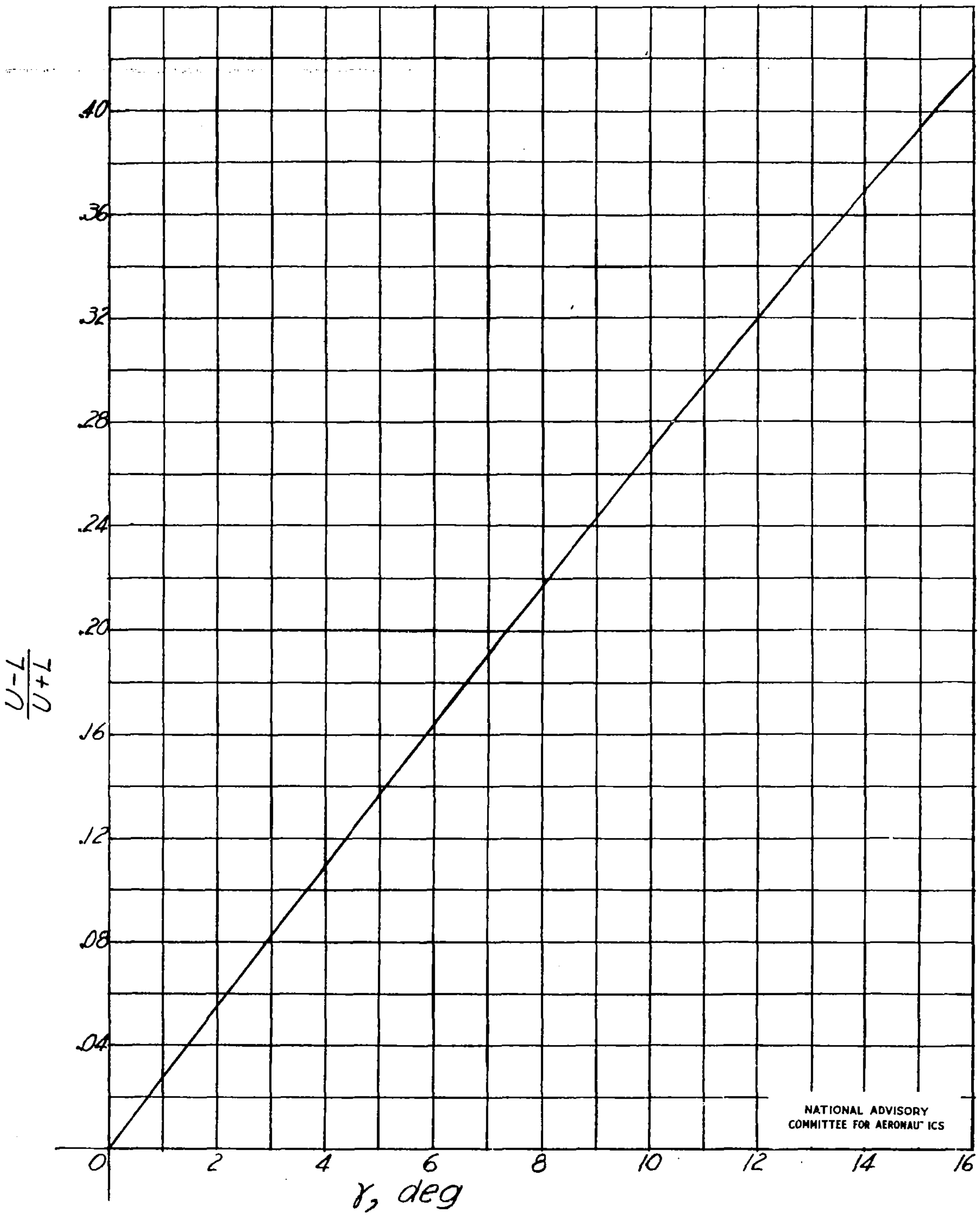

Figure 8.- Determination of $\gamma = \alpha + \beta_T$.

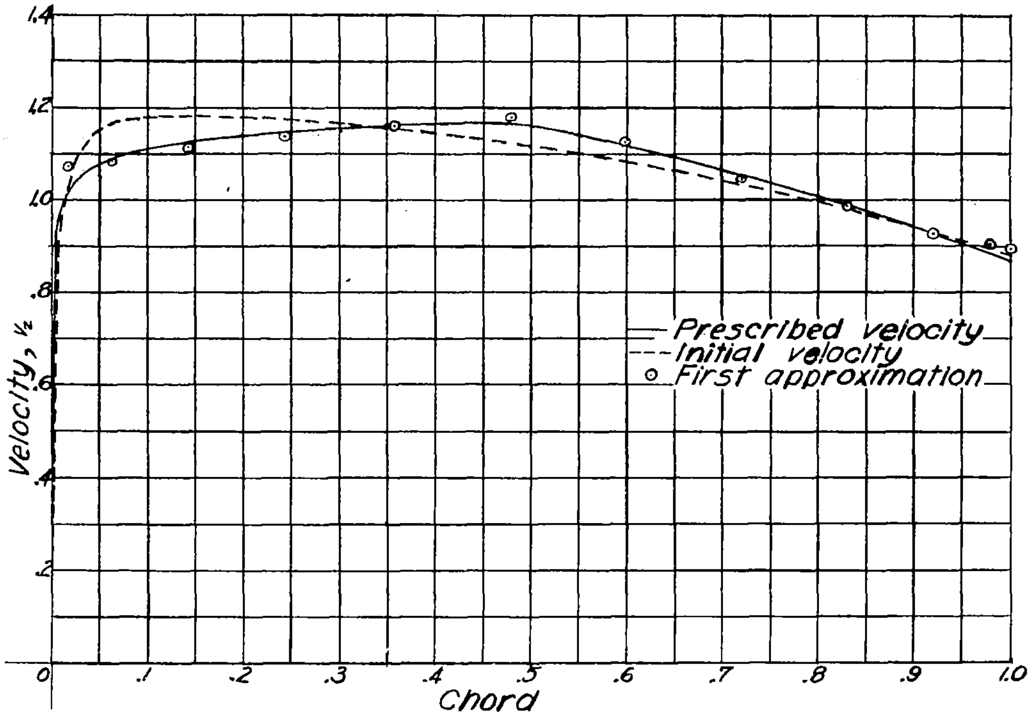

(a) Velocity distributions.

NATIONAL ADVISORY COMMITTEE FOR AERONAUTICS

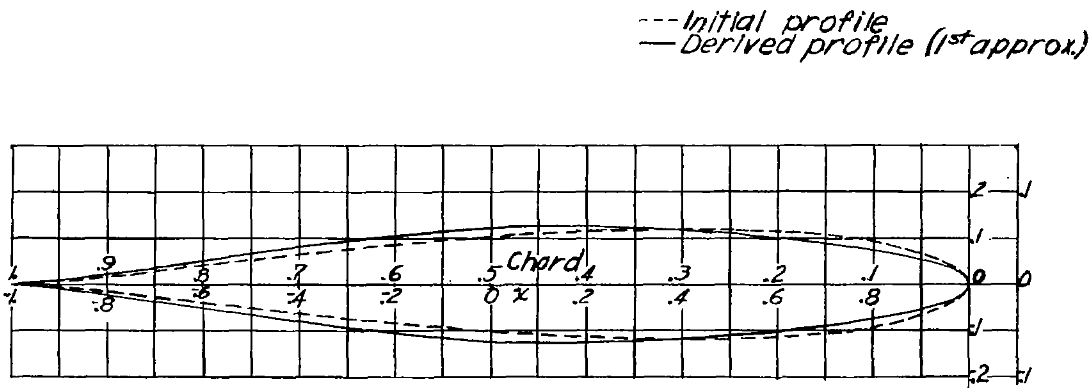

(b) Profiles.

Figure 9.- Inverse CMF method for basic thickness form.

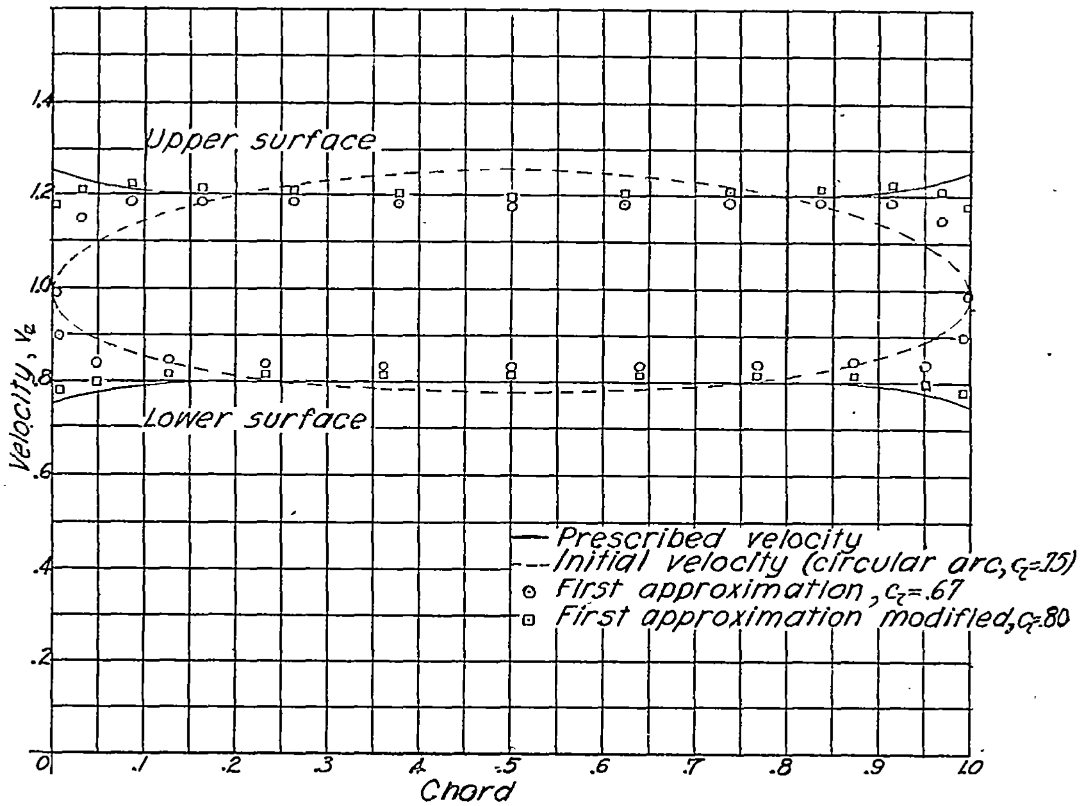

(a) Velocity distributions.

NATIONAL ADVISORY COMMITTEE FOR AERONAUTICS

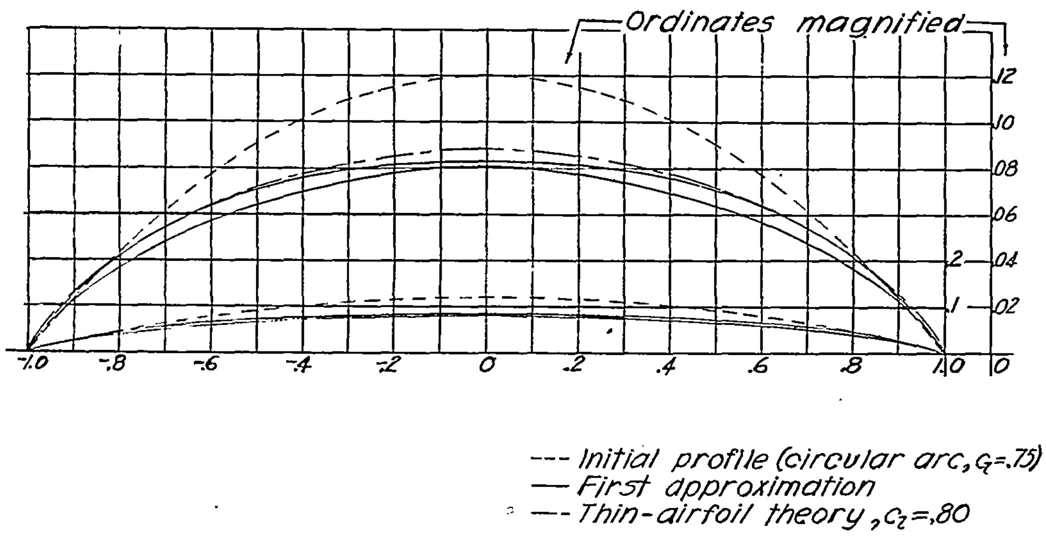

(b) Profiles.

Figure 10.- Inverse CMF method for a=1 camber line, c_l=0.80.

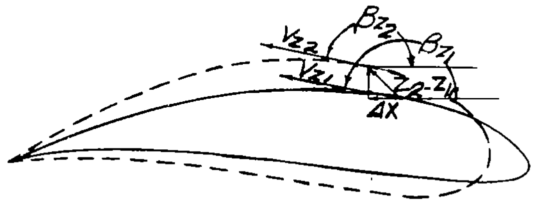

Figure 11.—The method of Betz.

NATIONAL ADVISORY
COMMITTEE FOR AERONAUTICS

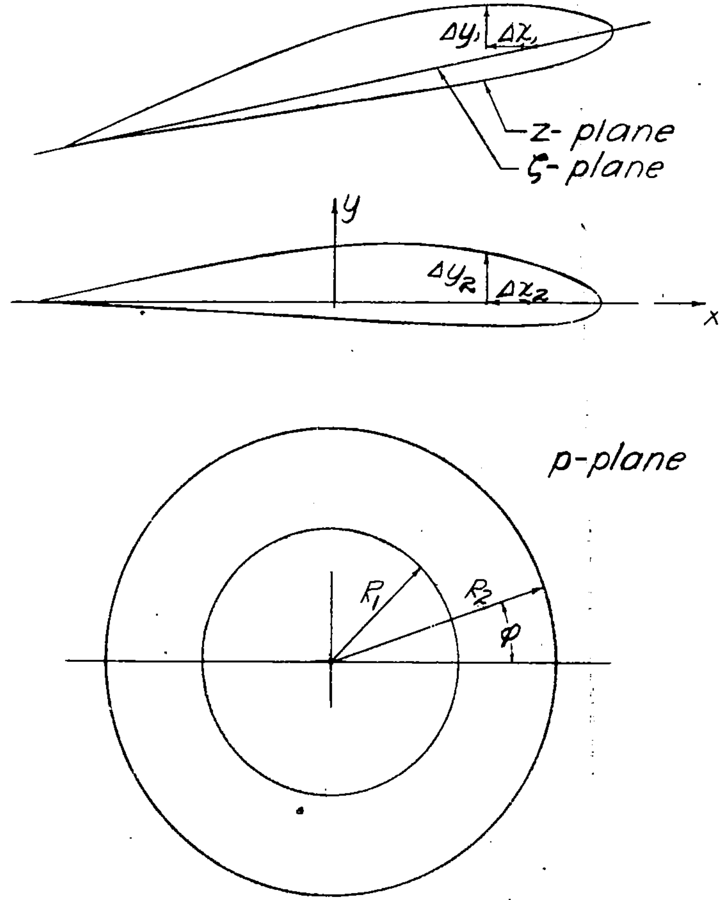

Figure 12.– Cartesian mapping function for biplanes.

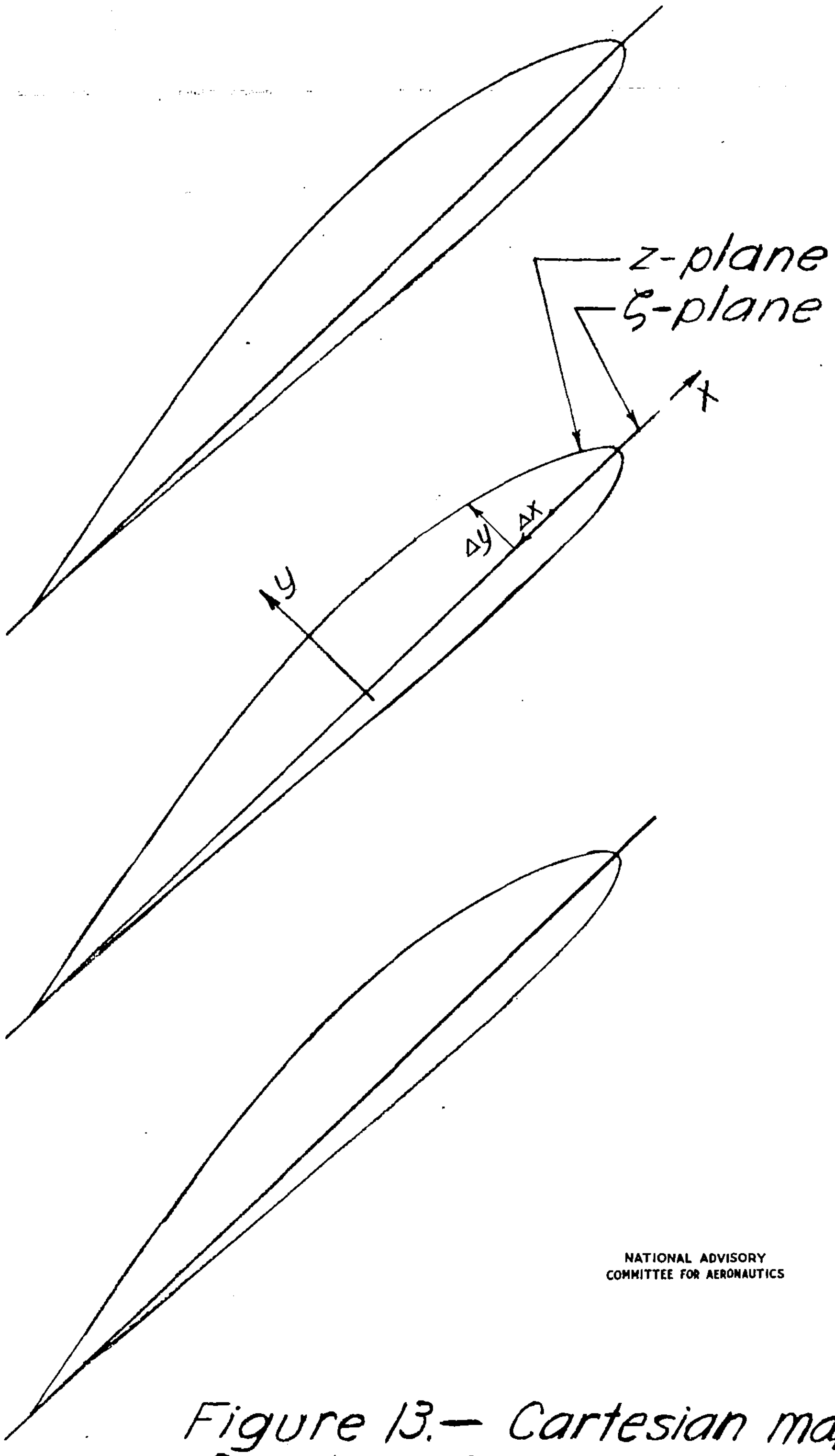

Figure 13.— Cartesian mapping function for cascades.

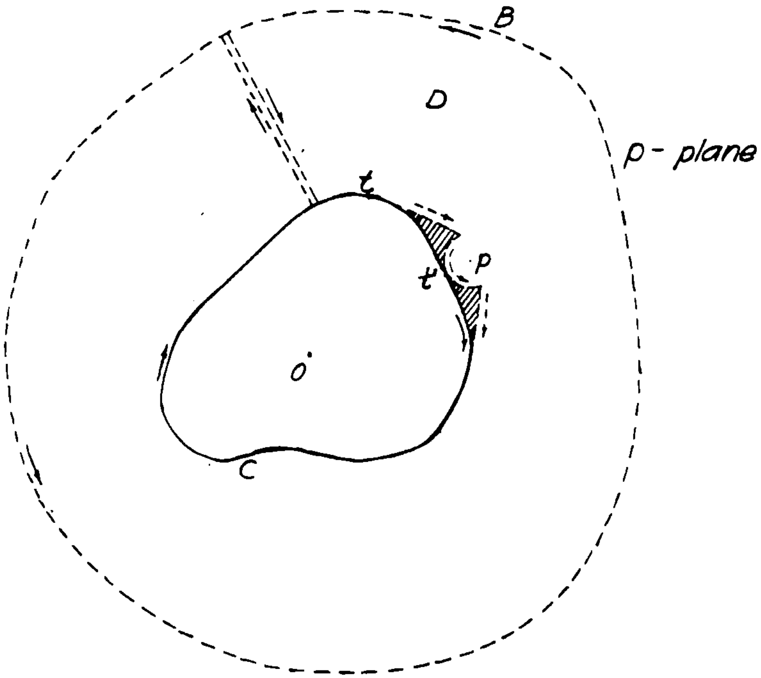

Figure 14.—Application of the Cauchy integral formula.

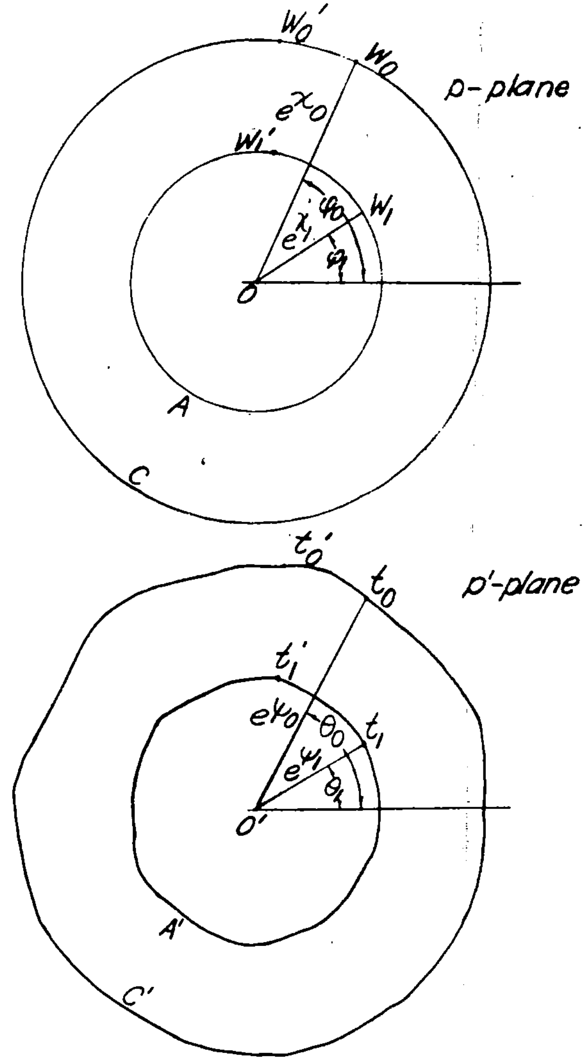

Figure 15.— Ring domains.